AN INVESTIGATION OF THE INFLUENCE OF VARIOUS EXPERIMENTAL PARAMETERS ON ELECTRON BOMBARDMENT MATRIX ISOLATION EXPERIMENTS

By

Kaitlynn Amanda King

A thesis submitted to the Graduate Program in Chemistry in conformity with the requirements for the Degree of Master of Science

Queen's University

Kingston, Ontario, Canada

April, 2015

Abstract

The products of d_6-ethane decomposition following charge-transfer ionization by Ar^+ are studied in the present thesis to understand the reaction mechanisms that occur in the electron bombardment matrix isolation apparatus. Gas mixtures of 1:1600 d_6-ethane:Ar were electron bombarded and the resulting ionization products, as well as remaining reagent molecules, were collected in a condensed matrix of argon. The products of ionization include the neutral dehydrogenation products C_2D_5, C_2D_4, C_2D_3, C_2D_2, and C_2D. These products are all observed in other studies completed at the same energy of 15.8 eV, save C_2D, but differ in their relative yields. Experimental parameters were explored in the present work, including relative flux of electrons, as well as relative density of electrons in the reaction zone.

Using two anodes of differing geometries, the density of electrons in the reaction zone was changed, creating either a low or high ion-density environment. Altering this parameter changed the observed product distributions. C_2D_4 and C_2D_2, were the sole two products observed under low ion-density conditions, whereas all of the products listed previously were observed under the high ion-density conditions, most notably the C_2D product. It is discussed that the observation of C_2D, following ionization of ethane at 15.8 eV, is indicative of the occurrence of dissociative recombination processes. The other reaction processes that occur from dissociative recombination are discussed. Under low ion-density conditions, where dissociative recombination does not occur, the distribution of products is more similar to other research at an ionization energy of 15.8 eV, however differ in the relative product ratios. This is justified based on differences in reaction timescales between the present experimental work and other work on the ionization of ethane.

Another experimental parameter, electron-flux, is investigated here and found to have a similar effect whether in low or high ion-density experimental conditions. The general trend is that as electron-flux increases, the extent of d_6-ethane precursor consumption increases as well. Increasing the electron-flux parameter under the high ion-density conditions causes a more significant increase in reagent consumption, as compared to the same increase in the same experiment completed using low ion-density conditions.

Acknowledgements

There are a number of people I would like to acknowledge for their influence and encouragement through this long journey that my thesis has become. From start to finish, I have met and worked with many influential people in a research, instructional, or employment capacity who have helped to shape the person that I have become. I want to thank the many knowledgeable professors and instructors at both Trent and Queens University who have taught me in either a classroom or laboratory capacity. Their dedication to teaching with integrity was very much appreciated.

I want to extend a huge thanks to Dr. J. Mark Parnis for his continuous and unwavering support from beginning to the, long-awaited, completion of a draft of this thesis. Your kindness, dedication, and understanding have always come when it was needed the most.

I want to thank the many members of the Parnis lab for their support over the years. I feel much gratitude towards Dr. Matthew G. K. Thompson for his monumental influence in my university career and the early years of my thesis work. A big thank-you also goes out to my colleagues Steve Walker, Matt White, Brandi West, Laura Prest, Bryan Linford, and Sasha Campbell for adding a little bit of fun into the long days in the lab.

The endless encouragement from my family, despite their lack of a full understanding of the subject matter I was working on, has always been appreciated. From the pride beaming from my late Grandads face whenever we discussed my work, to the curiosity and thoughtful comments from my daughter, family has always been a bright light in my life that pushed me forward when things seemed difficult.

Table of Contents

List of Figures

List of Schemes

List of Tables

List of Abbreviations

EBMIS	**Electron bombardment matrix isolation spectroscopy**
EI	**Electron ionization**
FTIR	**Fourier transform infrared spectroscopy**
IR	**Infrared spectroscopy**
PEPICO	**Photoelectron photoion coincidence spectroscopy**
QET	**Quasi-equilibrium theory**
RRKM	**Rice-Ramsperger-Kassel-Marcus**
UV-VIS	**Ultraviolet-visible**
VUV	**Vacuum-Ultraviolet**

Chapter 1

Introduction

1.0 – Overview

A central part to chemical research is understanding processes that occur following the ionization of a molecule in the gas phase. During ionization, energy is transferred to a species and distributed throughout the molecule, usually causing structural changes. Gas-phase ion chemistry has been studied for many years and applied in areas such as structure determination, unimolecular dissociation, and ion-molecule reactions, to name a few[1]. For example, studies that examine the decomposition of ionized hydrocarbons are important in an environmental sense since they may act as models of stratospheric decomposition for molecules that pass through the troposphere[2]. To mimic such an application, it is important to be able to study the decomposition of these molecules in the gas-phase, where the chemistry of the single molecule is observed, un-perturbed by solvents or the surroundings. The elucidation of the decomposition mechanism of an ion, along with the identification of any potentially reactive intermediates, is important for atmospheric applications as well as understanding the physical properties of the molecules and ions in our world.

Recent studies within our laboratory have demonstrated that processes other than the expected simple, unimolecular ion decomposition occur during the Electron Bombardment Matrix Isolation Spectroscopy (EBMIS) experiments. The processes that occur depend on experimental variables such as partial pressure at the reaction site, as well as the ionizing electron current. In one study of acetone ionization and decomposition, increasing the acetone:Ar mole ratio of the gas sample was shown to encourage ion-molecule reactions, as a result of increasing the partial pressure of acetone in the ionization region[3]. This study provided

an explanation for the observation of products other than those expected from unimolecular decomposition. The expected unimolecular decomposition products, however, were also not observed in the lowest mole ratio experiments, where ion-molecule reactions are minimized. Some of the main products were C_2H_6, C_2H_4, C_2H_2, C_3O, and CO and were rationalized through a mechanism where secondary ionization events of ethane were proposed to lead to the sequentially dehydrogenated products, which are summarized as follows in Scheme 1.

Scheme 1: General scheme of resulting products following subsequent charge-transfer ionization, via Ar^+, and neutralization in the matrix of the sequentially-produced dehydrogenation products of ethane, a main product of acetone ionization in the EBMIS apparatus.

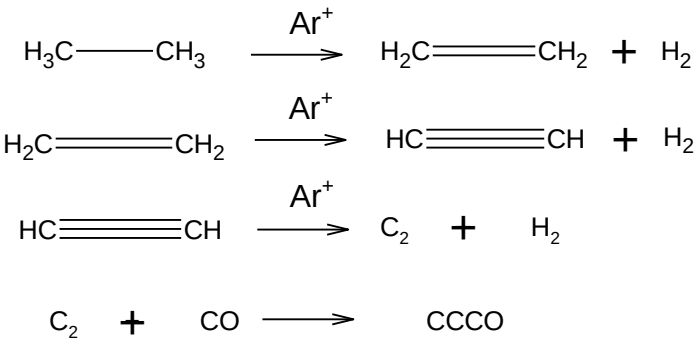

Overall, the aim of the current project is to investigate the effects of various experimental parameters on the ionization mechanism, as manifested through the products observed in the EBMIS apparatus. The project begins by re-investigating the occurrence of secondary ionization in our EBMIS apparatus by simplifying the starting reagent to ethane, and observing the effect of varying the electron-flux on products identified in the Fourier Transform Infrared (FTIR) spectra. A new parameter that affects product distribution, ion density, is also identified here, and the effects of a related experimental modification are examined. The clarification of how

these parameters affect the observed products, and therefore the reaction pathways that occur in our EBMIS experiments, will allow experiments to be tuned to allow access to a variety of different ionization reaction pathways.

1.1 – Concepts of Gas-Phase Chemistry

Chemical processes that are studied in the gas phase have the benefit of simplicity, compared to those studied in solution, as molecules in the gas phase are isolated from one another. A gas-phase chemical reaction provides the opportunity to observe changes that occur in a single molecule following a unimolecular process. While the occurrence of bimolecular process cannot be completely ruled out in EBMIS experiments, unimolecular chemistry is expected to explain the majority of the processes that occur. As such, the concepts of unimolecular, gas-phase chemistry are of relevance here and will be discussed in the following section.

The basic theory of unimolecular kinetics is explained by Rice–Ramsperger–Kassel–Marcus (RRKM) theory and/or Quasi Equilibrium Theory (QET). RRKM theory describes the rate constants associated with unimolecular reactions as a function of internal energy. In general, the expressions for both RRKM and QET methods are based on a system's excess energy that is available for reaction, following ionization. Rate expressions based on RRKM theory are expressed in terms of the excess energy available to an ion, which changes with the critical energy of the system, and in terms of factors that attempt to account for the bonding properties of an associated transition state. Reviewing further details of RRKM theory is beyond the scope of the present work, but a discussion of such can be found in the monograph by Robinson and Holbrook[4].

The somewhat simplified assumptions of QET can be used to describe the nature of unimolecular reactions and help to explain observed products. The details of these assumptions are described by Gross[5] and reviewed by Lorquet[6], Brenton *et al*[7], and Rosenstock *et al*[8]. An overview of the general concepts relating to the origins of decomposition will be covered here. QET shows how the rate of a unimolecular reaction depends on the available internal energy and how that energy is distributed throughout the molecule as vibrational energy. The basic assumptions of QET explain that, during ionization, energy will distribute randomly throughout the molecule. The probability of each energy distribution determines which products will be observed.

To begin understanding the physical aspects of decomposition, a few concepts should be reviewed. Firstly, upon ionization, the molecular geometry of an incipient ion remains unchanged as a result of transitions occurring vertically, instead of adiabatically. This is explained through both the Born-Oppenheimer approximation and the Franck-Condon principle. The Born-Oppenheimer approximation articulates that nuclear motion can be considered slow in comparison to electronic motion, which is effectively instantaneous[5]. In assuming that nuclear motions are slow, the vibrational modes of a molecule can be ignored when considering its initial geometry in this ionized state. This is stated using the Franck-Condon principle that says the nuclear coordinate positions of the atoms within the formed ion will initially remain the same upon ionization during an electronic transition to a new potential energy surface[5]. The potential energy surface of newly formed cations are composed of a continuum of low-lying excited electronic and vibrational states. Transitions will occur between these states following the initial vertical transition.

Given that the low-lying states are so close in energy, the transitions will occur quickly, allowing the energy to randomly distribute as vibrational energy prior to the molecule fragmenting in any way. The rearrangement and dissociation patterns are determined by the probabilities of these energy rearrangements for a particular molecule of interest. The final distribution of products depends on these patterns, as well as the total energy imparted to the ion itself. It is possible to observe subsequent dissociation of the initial products of ionization if an ion retains sufficient internal energy after undergoing an initial fragmentation.

1.1.2 – Unimolecular Ion Decomposition: Mass Spectrometry Concepts

The unimolecular decomposition of ionic species has been studied over the years using, predominantly, mass spectrometric techniques[5]. Mass spectrometry is a well-known tool that can be used for studying gas-phase ions and their decomposition patterns, following ionization. Various methods for ionization have been developed in order to perform either electron ionization or one of the various types of chemical ionization[5].

The original method of ionization in a mass spectrometric experiment, electron ionization, has been reviewed extensively in the literature[9]. Electron ionization occurs when a high-energy electron impinges on a neutral species, transferring some of its energy. If the transfer of energy is sufficiently greater than the ionization energy of the species, ionization will occur as follows;

$$M + e^- \rightarrow M^{+\cdot} + 2e^- \qquad (1)$$

A radical-cation, $M^{+\cdot}$, is produced, the fate of which depends on the internal energy that remains after its formation. If the transferred energy exceeds the ionization energy of the species, this excess energy will be distributed through translational, rotational, vibrational or

electronic degrees of freedom. Most of the energy will be stored as vibrational or electronic energy, generally causing fragmentation when the vibrational energy is great enough. Typically, electron ionization will result in extensive fragmentation, the products of which will vary depending on the extent of vibrational excitation, resulting from the transfer of excess energy. Ions will often fragment in characteristic ways, such as the loss of a molecular hydrogen unit, or methyl group. These cleavage patterns, covered extensively by Gross[5], represent typical decomposition pathways, but variations occur occasionally. For example, the cleavage reactions of amine radical cations change, depending on the size of the molecule, since a larger molecule will have more degrees of freedom in which to distribute internal energy[10].

Recently, the chemical ionization method has become one of the more widely-used modes of ionization. Chemical ionization has been termed a softer ionization since it usually involves transferring less energy to the molecule than in electron ionization, and therefore causes less extensive fragmentation or none at all. A molecular species can be ionized through chemical ionization in four characteristic ways: proton transfer, electrophilic addition, anion abstraction, or charge transfer. Charge-transfer ionization, where a neutral molecule is ionized through the interaction with an ion, is most relevant to this work and described by the following equation:

$$X^{+\cdot} + M \rightarrow X + M^{+\cdot} \qquad (2)$$

The ionizing species, $X^{+\cdot}$, initially formed through a method such as electron ionization, subsequently recaptures an electron from a neutral molecule, thereby ionizing that same molecule. This newly ionized molecule, $M^{+\cdot}$, is left with an internal energy described by:

$$E_{M+\cdot} = EA_{X+\cdot} - IE_M \qquad (3)$$

where the EA is the electron affinity of the $X^{+\cdot}$, and IE is the ionization energy of the molecule being studied. This excess internal energy causes an increase in vibrational motion, which

usually leads to the fragmentation of the molecule in a variety of ways. Charge transfer will successfully occur for a reaction where the energy difference from Equation 3 is negative, meaning that there is an excess of internal energy. If it is only slightly so, the majority of the ionized species will be observed as the molecular ion, $M^{+\cdot}$, but fragmentation will begin to occur as the excess internal energy increases. With that in mind, a large difference between these two values will increase the expected extent of decomposition.

The assumptions of QET propose that further decomposition of the initially formed products may occur if the ion has excess energy following the initial decomposition step. The various reaction pathways that exist may be studied using different methods to investigate the products of reactions completed at various energies. One of these methods, photoelectron photoion coincidence spectroscopy (PEPICO), is discussed in more detail in the next section.

1.2 – Photoelectron-Photoion Coincidence (PEPICO) Spectroscopy

Photoelectron-Photoion Coincidence Spectroscopy (PEPICO) describes a type of experiment that uses mass spectrometric detection to study the decomposition of ionized molecules as a function of internal energy. A mass spectrometer, usually employing time-of-flight (TOF), analyzes ions that are produced through photoionization and detected in coincidence with a corresponding electron, of measured kinetic energy. PEPICO studies investigate ion decomposition at precisely determined internal energy values in order to produce breakdown curves for a particular reagent molecule[11]. Branching ratios for each competitive decomposition pathway are shown in these breakdown curves, at various internal energies.

There are, generally, two different kinds of PEPICO experiments that can be used. In the first, a fixed light source is used for photoionization, and ions are selected based on the collection

of electrons of a particular energy. The second approach, which is more widely used today, is called Threshold PEPICO (TPEPICO), where photons of known energy are used for ionization and subsequent ions are measured in coincidence with the collection of zero-kinetic-energy electrons. The photon energy is sequentially varied and the branching ratios of ions at each energy level are determined. This TPEPICO technique provides accurate determinations of the appearance energies of corresponding ions, with resolutions of less than 5meV.

With the ability to accurately select for ions of a particular energy, PEPICO can examine decomposition patterns and rates, which prove to be useful as a reference point for other studies. The energy required for the onset of production of each decomposition product of a particular ionized molecule is determined through PEPICO experiments, which can help to predict what products would be expected for experiments conducted at particular energy levels.

Products observed in the EBMIS work are similar to those found in mass spectrometry, given that both study decomposition products following ionization events. The EBMIS experiments relate closely to PEPICO studies within an internal energy range that matches that which is transferred to the molecule following efficient charge-transfer ionization. For this reason, EBMIS experiments could be used in the future to complement PEPICO studies, providing a complementary tool for structural identification.

1.3 – Matrix Isolation

The matrix isolation technique was proposed by Pimentel *et al*[12] in 1954 in order to study reactive or unstable substances. The technique was intended to trap reaction products within an inert solid matrix, at cryogenic temperatures, in order to isolate them from one another and

inhibit further reactions. A schematic diagram, illustrating this idea of trapping species in a matrix, is shown in Figure 1.

In early matrix isolation experiments, relatively warm temperatures were used to form matrices, where the lowest temperature reached was 66K, allowing some materials to successfully solidify and some remained soft. Soft matrices allow for movement and diffusion of small molecules and therefore are not effective at trapping most species. Matrix materials that are transparent in the infrared, such as the noble gases, are preferred, however some of the initial materials used such as CO_2 and CCl_4 were used with some success since their infrared spectra are well known and have broad gaps where there is no infrared absorption. It was also noted in this first description of the matrix isolation method that the mole ratios, of matrix material to reagent, need to be 100 or larger in order to prevent recombination reactions.

With the development of better cryostats through the 1950s and 60s, colder temperatures were obtainable, which allowed for the use of other matrix materials. In 1966, Andrews and Pimentel reported isolating lithium nitroxide, LiON, in an argon matrix[13]. This experiment was conducted at about 15K, a temperature which will allow many matrix-forming materials to be used. In the early 1970s, organic chemists began using the matrix-isolation technique and collectively characterized cyclobutadiene, isolated in argon, using different precursors[14]. The mechanism had been apparently studied extensively in the past, but the matrix isolation experiment provided exclusive evidence for parts of the mechanism, by examination of the molecules, frozen in time. The structure of cyclobutadiene was finally deduced in 1978, using an Argon matrix at 7K, by examining the details of the infrared spectrum.

Methods for generating reactive species can vary in each matrix experiment, so products can either be produced before or after the solid matrix is formed[15]. Firstly, precursor molecules

diluted in matrix material can be initially deposited onto the cold substrate, followed by the initiation of a reaction by irradiation. Alternatively, reactive species may be generated prior to deposition by some method such as excitation by photons, pyrolysis, or electronic excitation. A method is chosen based on the type of study being completed, since effective study of different reactions will depend on whether they occur before, rather than after, the formation of the matrix. For example, if the study of a reaction in the gas-phase is desired, as is relevant to this work, the reaction is conducted above the cold substrate and before matrix condensation. In these types of experiments, products are formed and are quickly isolated as condensation occurs, quenching any further reaction or decomposition. If, however, a photolytic experiment is being performed, irradiation can be performed after matrix formation to provide energy to molecules isolated within the matrix.

Various matrix effects need to be considered when interpreting the results of a study, depending on the nature of the material and temperature conditions used[15]. Interactions between the trapped species and the matrix material may occur depending on whether an inert noble gas is used, or a mildly reactive gas. The physical restrictions of molecules that are isolated in a matrix may need to be considered, especially if a structural technique like infrared spectroscopy is used, since the spectra will be different when rotation is inhibited. The specifics will be covered in the section describing the infrared spectroscopic technique. The influence of cage effects on the observed reaction pathways is very important to consider, since low-temperature matrices will naturally form relatively rigid cages. If the matrix is condensing during the decomposition of a molecule, and both fragments become trapped in the same cage, they may simply recombine to form the original molecule because of their close proximity.

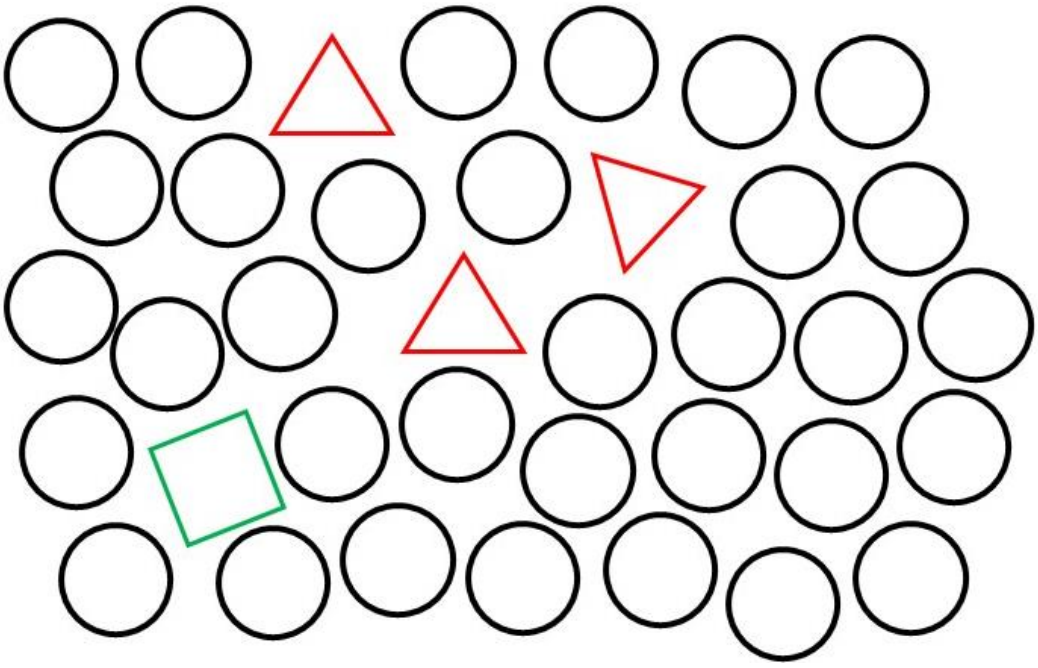

Figure 1: A schematic diagram illustrating how chemical species become trapped in a condensed host-gas, such as Argon, which is represented here by the black circles. The trapped, or isolated, chemical species are represented here by the red triangles and green square.

Matrix isolation experiments today can be used to study short-lived species, or more specifically, test proposed reaction mechanisms by studying intermediates and characterizing weak interactions between complexes. Once trapped in a condensed matrix, a detection method is needed that will analyze the products isolated in an undisturbed environment. Matrix isolation techniques are used in the current work, along with using infrared spectroscopy for identification.

1.4 – Fourier-Transform Infrared Spectroscopy

Fourier-Transform Infrared Spectroscopy (FTIR) is a technique used for structural characterization that is very useful for chemical identification. The benefits of using FTIR in conjunction with matrix isolation techniques is discussed at the end of this section. The basis of this type of spectroscopy are the vibrational modes of a molecule, oscillating at unique energies. A non-linear polyatomic molecule of N atoms will have 3N-6 vibrational modes (3N-5 for a linear molecule)[16]. During infrared spectroscopic experiments, vibrational modes will be excited in a distribution reflecting the individual oscillator strengths of each vibration. The transmittance of infrared radiation through a sample is measured, which indirectly allows for the observation of the frequencies that are absorbed by a particular molecule. Each vibrational mode will absorb a characteristic amount of energy, E_{vib}, corresponding to a specific frequency of infrared radiation as described by the Bohr frequency condition,

$$E_{vib} = h\nu_{vib} \qquad (4)$$

where h is Plancks' constant and ν_{vib} is the frequency of a particular vibration.

Infrared radiation describes the portion of the electromagnetic spectrum from the edge of the visible spectrum at 700nm, through to 1mm, which corresponds to an energy that may impart

vibrational excitation throughout the bonds of a molecule. A molecule will absorb a photon of a particular energy if it matches the frequency, ν, of a quantized vibrational oscillation of atoms in the molecule. Molecular vibrations will correspond to either a stretching, bending or more complex deformation motion of a bond, any of which change the orientation of the atoms with respect to one another. When a particular motion results in a change in dipole moment of a molecule, the molecule can interact with the oscillating electric field of the infrared radiation.

The vibrational energy or frequency of a given stretch can be approximated by treating the two atoms involved as a diatomic harmonic oscillator. Taking into account the masses of the two atoms involved in a particular stretching motion, Hooke's Law can be used to calculate the energy of infrared radiation that would be absorbed[17], using the equation as follows;

$$\bar{\nu}_s = \frac{1}{2\pi c}\left(\frac{k}{\mu}\right)^{1/2} \qquad (5)$$

where $\tilde{\nu}$ is the wavenumber, c is the speed of light, k is the force constant of the particular stretch, and μ is the reduced mass ($\mu = m_a m_b / m_a + m_b$) for two nuclei involved in the particular stretch. Infrared frequency information is typically displayed as a wavenumber, $\tilde{\nu}$, in units typically ranging from 4000 to 400 cm^{-1} , which is related to frequency, ν, as follows,

$$\bar{\upsilon} = 1/\lambda = \nu/c \qquad (6)$$

where λ is the wavelength of light in cm, and c is the speed of light in cm/s. Equation 5 shows that the frequency of a vibrational mode depends on both the reduced mass of the two atoms involved, as well as the force constant of that bond. Based on those two parameters, generalizations can be made about over what range of the spectrum various types of stretches are likely to be observed. For example, the C-H stretch of an alkane is expected to be observed between 2800-3000 cm^{-1}, whereas the same type of stretch in an alkene is predicted between

3000-3100 cm^{-1}. There is a larger difference between vibrational modes when considering different functional groups, such as C=O or O-H stretches, which makes infrared spectroscopy a powerful tool for structural identification. Within a functional group family, each molecule will have a unique vibrational mode, since the exact energy that is absorbed depends on the interactions of the simplified diatom with the other portions of the molecule. Other molecular motions such as bending and deformation vibrations are less easily predicted and are typically used simply as an additional fingerprinting tool, usually observed at the lower energy of 1300-400cm^{-1}.

There are factors of vibrational motion that complicate infrared spectra when a sample is in the gas phase that cause spectral broadening. The broadening of vibrational modes occurs as a result of coupled interactions with neighbouring atoms. When FTIR is used in conjunction with matrix isolation techniques, clear spectra are generated that are more easily interpreted. This clarity comes as a result of working at very low temperatures, in which there are physical restraints on the matrix isolated species. Rotational movement of a species is minimized in a matrix cage, resulting in the elimination of the rotational fine structure that arises in gas-phase infrared spectra, resulting in narrow bands that are more resolved. This effect will increase the signal to noise ratio in the spectrum and reduce spectral overlap of modes and therefore allow for better identification. The combination of MI and FTIR techniques can be used to investigate ion chemistry, especially in cases where a product has a short lifetime.

Chapter 2

Literature Review

2.0 Background of the EBMIS apparatus

Prior to using electron bombardment as an ionization method, matrix isolation experiments were coupled with such methods as vacuum-ultraviolet photolysis, reactive atomic sources, lasers and radiolysis. Each of these methods can be used to energize a molecule of interest and generate fragments to be matrix isolated and subsequently analyzed. The products resulting after a particular ionization technique may vary, depending on the method and amount of energy transferred.

One of the benefits of using electron bombardment as a method of ionization is that the parameters of the experiment, including electron flux and energy, are easily tunable. The benefits of using electron bombardment to ionize a substrate was realized in the work by Milligan and Jacox[18] in 1970 when an electron gun was used to ionize NO_2. In these studies, the NO_2^- molecular ion was isolated following ionization by electron bombardment, vacuum-ultraviolet photo-ionization, or alkali-metal photo electrons. Electron bombardment occurred concurrently with deposition onto the cryogenic window. An electron beam was generated from heating a tungsten filament, which was biased to 300V, to generate a beam in which the gaseous sample would pass through[18].

It was reported in another study that electron bombardment of neutral metal-carbonyls, $Ni(CO)_3$, $Cr(CO)_5$, and $Fe(CO)_4$, resulted in very similar, if not identical, spectra compared to the other ionization methods that had been used, such as the common visible-ultraviolet photolysis[19]. The ionization products were trapped in 10 K matrices and identified by infrared analysis after

electron bombardment, and VUV-photolysis. Two possible mechanisms of ion formation following electron bombardment were suggested in this work, which are as follows[19]:

1. Electron capture by a neutral molecule: $A + e^- \rightarrow A^-$ (7)
2. Dissociative electron capture: $A\text{-}CO + e^- \rightarrow A^- + CO$ (8)

A variety of studies are important to mention from the early years of coupling electron bombardment with matrix isolation, as the benefits and variety of applications became increasingly evident. In 1983, Knight *et al.*[20] reported the successful production of positive ions, $^{14}N_2^+$ and $^{15}N_2^+$, in a matrix using the electron bombardment technique coupled to electron spin resonance (ESR) experiments. It was noted that using electron bombardment to produce charged and radical species during deposition, allows for the study of a greater number of chemical reactions. This research group went on to isolate H_2O^+, and $^{13}CO^+$ cations, characterized by ESR spectra in other experiments.

In 1988, Suzer and Andrews[21] also reported some important initial work with H_2O that combined electron bombardment ionization methods with the matrix isolation technique. An infrared (IR) spectroscopy spectrum following these was recorded to examine the influence of this new combination of ionization and capture techniques. Differences in the nature of products were analyzed in order to point out the various reactions that could occur as a dilute mixture of reagent water vapour in argon was bombarded by electrons. The IR characterization of OH^- and OH radicals was reported for the first time as a result of these experiments. Discussions of the 'soup' of reactions that are possible ensued with considerations of the primary (fast) electrons as well as the secondary (slow) electrons that float around the matrix as a result of primary ionization. The proposed reactions are shown in Scheme 2, as follows.

Scheme 2: A list of the multiple reactions available during an electron bombardment experiment with either a primary electron, a slow, secondarily-produced electron, or an ionized argon atom[21].

e^- (primary) + H_2O → OH + H + e^- (slow)

e^- (primary) + Ar → Ar^+ + $2e^-$ (slow)

e^- (primary) + Ar → Ar^* + e^- (slow)

e^- (slow) + OH → OH^-

e^- (slow) + H_2O → H^- + OH

Ar^* + H_2O → Ar + OH + H

Ar^* + H_2O → Ar + 2H + O

Ar^+ + H_2O → ArH^+ + OH

After this initial work, Suzer and Andrews used this electron bombardment technique to study CCl_4, in which a 400/1 sample of Ar/CCl_4 was bombarded with 100eV electrons produced from a heated tungsten wire[22]. The dominant products were CCl_3, CCl_2, CCl_4^+, CCl_3^+ and Cl_3^+, and a higher yield of the neutral products were observed with an increase in electron energy. Further work by this group, using NH_3, considered the fate of the eminently present secondary electrons within the matrix. The identification of ionic species was attributed to dissociative attachment of the precursor NH_3 or H_2O on the surface of the matrix.

The electron bombardment matrix isolation apparatus constructed by Szczepanski *et al.*[23] in 1992 was constructed so that reactions would occur in the gas phase, prior to condensation as a matrix. Given that the apparatus used for the present work was modeled after the apparatus used by Szczepanski *et al.*[23], a description of this important work is appropriate here. Their work

was focused on obtaining the infrared spectrum of naphthalene, a polycyclic aromatic hydrocarbon. Argon gas was used as the carrier gas, in which an addition of CCl_4 was also used to enhance ionization during electron bombardment. The apparatus was constructed with an anode near the matrix deposition window so that an electron beam, produced from a heated tungsten filament, would interact with a stream of gas just above the window. The reason for the construction was to have the naphthalene ionized in the gas-phase, rather than a condensed phase. The ionization process that was proposed involved charge-transfer to naphthalene from ionized argon to create the naphthalene cation, as follows:

$$Ar + e^- \rightarrow Ar^+ + 2\ e^- \qquad (9)$$

$$Ar^+ + Nap \rightarrow Nap^+ + Ar \qquad (10)$$

with the possibility of charge transfer with CCl_3^+, the product of CCl_4 ionization, as follows:

$$CCl_4 + e^- \rightarrow CCl_3^+ + Cl + 2e^- \qquad (11)$$

$$CCl_3^+ + Nap \rightarrow CCl_3 + Nap^+ \qquad (12)$$

The factor of relative concentrations of each species was also discussed when considering the probabilities of the various ionization processes available. Given that argon is the most prevalent gas in the mixture, it is most likely that it will be ionized directly by the high-energy electrons, and subsequently ionize any molecule found in lower concentration, here being the naphthalene molecules. The same concept holds true in the present work, which becomes important when considering assigning products and corresponding reaction processes.

2.1 Background of Matrix Isolation and EBMIS work in the Parnis group

Prior to the construction of the EBMIS apparatus, the Parnis group studied the interactions of small organic molecules within a formed matrix via other methods than electron

bombardment. The vibrational spectrum of the acetone-water complex was studied by co-deposition onto a 12 K spectroscopic window using different ratios of analyte to matrix gas[24]. Correspondingly, these matrices were characterized using FTIR spectroscopic methods. The shifts that were noted in this study demonstrated that matrix isolation combined with FTIR detection is sufficiently precise to give information about dimerization and other such interactions within the matrix environment. Given the sensitivity observed in the shifting of vibrational features in these experiments, this method was deemed successful in trapping reaction intermediates, or unstable product species.

Reactions of $O(^1D)$ with small hydrocarbons were studied by Parnis *et al.*[25] using broad-band ultraviolet-visible (UV-VIS) irradiation of condensed matrices in order to study the photoionization of such molecules. Gaseous samples containing 2% N_2O and 10% hydrocarbon (CO, CO_2, CH_4, ethane, propane, or isobutane) in argon were studied via co-condensation and subsequent FTIR analysis. Upon irradiation of these hydrocarbons within the matrix, the corresponding primary alcohols were found to be the major products, suggesting that the products were quickly stabilized within the matrix.

This earlier work was supportive evidence of the effectiveness of the constructed matrix isolation apparatus at trapping primary reaction products with an inert matrix. The next desirable step was to redesign the apparatus to undergo ionization in the gas phase prior to condensation onto the window. It was thought that this work would complement mass spectrometric data, as short-lived species that may be subject to decomposition in a gaseous mass spectrometric experiment, would be trapped and isolated in the matrix environment. Adapting from the Szczepanski *et al.*[23] work, an electron bombardment matrix isolation apparatus was constructed in the Parnis laboratory. In 1997, Zhang *et al.*[26] published the early EBMIS work in the Parnis

group that investigated isomerization and decomposition products of ionized acetone. This electron bombardment method of ionization was adapted to investigate gas-phase ionization, while using the matrix isolation method to isolate the resulting products. A major focus of the work was regarding the production of the isomerization product, 1-propen-2-ol, or the enol isomer of acetone, as well as the decomposition products, $CH_3CO^{\bullet}$, CH_2CO, CH_4, and $CH_3^{\bullet}$. From this work, mechanisms that were identified as dominating in this system include isomerization (to produce the enol isomer) and decomposition following ionization of the precursor acetone molecule. It was also noted that neutralization processes, through electron capture, were prominent since cationic products were not observed. This work suggested an abundance of electrons in the vicinity of the cold-substrate window during condensation. Given this abundance of electrons, a variety of reactions could occur prior to formation of the matrix depending on how far from the cold-substrate window the ions are created.

Other early work with this EBMIS apparatus included an investigation into the gas-phase ion chemistry of oxalyl chloride, $C_2Cl_2O_2$, by Fridgen and Parnis[27]. In such work, dilute mixtures of oxalyl chloride in a rare gas, either argon or krypton, were subjected to electron bombardment and the ionization products as well as any remaining precursors were matrix isolated. Following FTIR spectroscopic analysis, the products Cl_2CO, $ClCO^{\bullet}$, CO, and CCl were identified. Given the abundance of electrons in the reaction area, these neutral products were expected and explained in context with known mass spectrometric experiments. The difference in mass spectra following charge transfer ionization, as opposed to direct electron ionization helped to discern the type of processes occurring in the EBMIS apparatus. It is accepted that in EBMIS experiments, direct electron ionization of the rare gas atoms would occur, given that they

are always the most abundant entity in the mixture. The processes following production of the ionized rare-gas were considered in this work.

In light of the observed products, Penning ionization was ruled out as a mechanism for ionization of the analyte. The notable metastable levels of argon that would result from Penning ionization are 11.5, 11.6, 11.7, and 11.8 eV above ground state, and any higher energy levels are known to radiatively relax into a lower energy state rapidly. These energies are too low to explain the observed C-C cleavage products, Cl_2CO and $ClCO^{\bullet}$. The observed products under the particular experimental conditions were best-explained when ionization of the precursor occurred through charge-transfer with the ionized rare gas. The ionization energy of argon is 15.8 eV and 14.0 eV for krypton, which leaves the ionized analyte ion with sufficient energy to undergo bond cleavage to produce the observed products. After 10.91 eV of the transferred energy is used to ionize the oxalyl chloride, there remains excess energy for the ion to undergo unimolecular chemistry, such as the C-C cleavage to produce $ClCO^{\bullet}$ and $ClCO^{+}$. The major product of these EBMIS experiments was $Cl_2CO^{\bullet+}$, which differs from mass spectra, where this is a minor product[28]. This was attributed to the charge transfer ionization process, which would provide the ion with sufficient energy (468 kJ/mol, or 4.95 eV) to overcome the thermodynamic barriers shown in the following equations,

$$ClOCCOCl^{\bullet+} \rightarrow CO^{\bullet+} + Cl_2CO \qquad \Delta_rH = 298 \text{ kJ/mol} \qquad (13)$$

$$ClOCCOCl^{\bullet+} \rightarrow CO + Cl_2CO^{\bullet+} \qquad \Delta_rH = 47 \text{ kJ/mol} \qquad (14)$$

These studies helped discern some of the gas-phase ion processes that occur in the newly constructed EBMIS, namely that the ionization process is through charge transfer from the rare gas host to the precursor being studied.

2.1.1 Recent Work in the Parnis Group: acetone and dimethyl ether work

Work relating to acetone decomposition within the EBMIS apparatus was revisited by Parnis *et al.*[3] in 2009 in order to explore various experimental parameters and their effects on mechanistic processes. The impact of total gas flow rate indicated that when this increases, the efficiency of ionization simply decreases. Varying the mole ratio of gaseous acetone:Ar had a more complex impact on the products observed. Parnis *et al.*[3] report that at low mole ratios, the chemistry observed was attributed to single-molecule, whereas at higher mole ratios the observed chemistry could result from two or more molecules of acetone. This results in a diverse mixture of chemical reactions since an ionized acetone molecule could encounter either a second ionized acetone, a neutral acetone, or any of the products of ionization. The reactions proposed for a single ionized acetone molecule are displayed in Scheme 3, below, as an explanation for the production of a neutral ethane molecule. The observation of apparent dehydrogenation products relating to ethane, as shown previously in Scheme 1, is of interest in the present work.

Scheme 3:

$$Ar^{+\cdot} + CH_3COCH_3 \rightarrow Ar + CH_3COCH_3^{+\cdot} \quad \textbf{(Charge Transfer ionization)}$$

$$CH_3COCH_3^{+\cdot} \rightarrow CH_3CO^{+} + CH_3^{\cdot} \quad \textbf{(Unimolecular dissociation)}$$

$$Ar^{+\cdot} + CH_3CO^{+} + CH_3^{\cdot} \rightarrow CH_3^{\cdot} + CO^{+\cdot} + CH_3^{\cdot} \quad \textbf{(Subsequent ionization process)}$$

$$[CH_3^{\cdot} + CH_3^{\cdot}] \rightarrow C_2H_6 \quad \textbf{(Radical Recombination)}$$

The above product species differ from the products observed in EI mass spectrometry experiments. The production of ethane, as well as its dehydrogenation products, has been attributed to the occurrence of secondary ionization of the primary products. This is revisited in the current work, working with ethane as the starting molecule to better understand the observed products.

Other studies were also completed using dimethyl ether as the reagent, in order to give more information on the diverse chemistry that occurs within the EBMIS apparatus[29]. Mechanisms were proposed that agree with the energy available to a species ionized via Ar^+ charge transfer ionization. Upon consulting the breakdown curves associated with an available energy around 15.8eV, the expected products resulting from allowed reactions would have been H_2COH^+, $CH_3^\bullet$, HCO^+, CH_4, CH_3^+, H_2CO. When some of the expected products were not detected using the EBMIS apparatus, differences between our experiment and the corresponding TPEPICO work were examined. The first difference in the EBMIS experiments that had been identified in the past is that the volume of secondary electrons is high in the reaction zone which leads to neutralization of charged ions. In addition to that, it was noted that the pressure nearing the matrix window is quite high, as a result of condensation of the matrix itself. Given these considerations, the mechanistic schemes shown below were proposed that take into account the initial dissociation of the dimethyl ether ion, as well as the evident neutralization steps and possible effects of the high-pressure conditions. First, to explain the absence of the H_2COH^+ and $CH_3^\bullet$ products observed in TPEPICO work, a scheme was proposed that includes the initial dissociation step that would produce the expected products, and subsequent neutralization and abstraction steps, which is shown in Scheme 4.

Scheme 4:

$CH_3OCH_3^{\bullet +*} \rightarrow H_2COH^+ + CH_3^\bullet$ (Dissociation)

$[H_2COH^+ + CH_3^\bullet] + e^- \rightarrow [H_2COH^\bullet + CH_3^\bullet]$ (Neutralization)

$[H_2COH^\bullet + CH_3^\bullet] \rightarrow H_2CO + CH_4$ (Abstraction)

$[H_2COH^\bullet + CH_3^\bullet] \rightarrow CO + CH_4 + H_2$ (CO formation)

This scheme accounts for the presence of CO and CH_4 in typical spectra, while still undergoing the dissociation that would be expected, given the energy transferred to the formed ion. If the neutralization step is expected to have an impact on the above dissociation step, it would also affect the other expected reactions, which are as follows:

$CH_3OCH_3^{\bullet +} \rightarrow CH_3OCH_2^+ + H^\bullet \rightarrow HCO^+ + CH_4 + H^\bullet$ AE = 14.00eV (15)

$CH_3OCH_3^{\bullet +} \rightarrow CH_3OCH_2^+ + H^\bullet \rightarrow CH_3^+ + H_2CO + H^\bullet$ AE = 14.90eV (16)

These reactions are expected to occur in the energy range of our experiments, however, electron capture of the cation would cause further reaction progression in all cases. Electron capture of the HCO^+ would cause dissociation as follows,

$HCO^+ + e^- \rightarrow HCO^{\bullet *}$ (electron capture) (17)

$HCO^{\bullet *} \rightarrow CO + H^\bullet$ (dissociation) (18)

resulting in the observation of CO, only, in the FTIR spectra. Regarding equation 16 from above, electron capture would energize the CH_3^+ cation, but the high pressure environment of the forming matrix could allow for the following proposed hydrogen atom abstraction process.

$$[CH_3^+ + H_2CO] + e^- \rightarrow \{CH_3^{\bullet *} + H_2CO\} \quad \text{(Electron capture)} \quad (19)$$

$$\{CH_3^{\bullet +} + H_2CO\} \rightarrow CH_4 + HCO^{\bullet} \quad (H^{\bullet} \text{ abstraction}) \quad (20)$$

These proposed steps explain the products observed in light of the expected reactions at the corresponding energy range that is possible in charge transfer from Ar^+, as well as under the high pressure environment of the reaction zone of the EBMIS apparatus. Interpretation of these results was pertinent to understanding the seemingly complex distribution of products observed following all EBMIS experiments completed in the Parnis lab.

The present work uses ethane, actually ethane-d6, to more precisely investigate the process of ionization and product formation typical of the EBMIS apparatus. The deuterated form of ethane is used here in order to ascertain that the identified products had come from a precursor ethane-d6, rather than any minor impurities containing H-atoms. Ethane is an ideal molecule to work with because of the simplistic single C-C bond, and tetrahedral sp^3 hybridization. This work was aimed at being able to better understand the rich chemistry that seems to occur in the experiments completed using this apparatus. Ionization of this small hydrocarbon, and subsequent decomposition, has some diversity that depends on the ionization methods used and the length of time before ion detection. It is thus important to review what is known about the chemistry of ethane in the gas-phase.

2.2 Gas-phase Chemistry of Ethane

Ethane is the simplest molecule with a carbon-carbon bond, alas it has been studied extensively in the past and often used as a model for chemical processes. The 50eV electron ionization mass spectrum for ethane, available in the NIST database, displays the expected features associated with the loss of H_2, H-atom, or CH_3 from the parent ion. Over the years, various types of theoretical and mass spectrometric studies have been used to characterize ethane ionization and its associated decomposition products[30].

Work relating to ethane, using the PEPICO spectroscopic technique has developed over the years and provided quantitative information about the ionization of this simple molecule, including branching ratios. Breakdown curves were presented by Stockbaeur[31] through the use of TPEPICO work, which showed the branching ratios expected at ionization energies ranging from 11-16 eV. This was important work in that it shows which products are expected to be observed following ionization at a particular energy. Their work showed that below 14eV, the available decomposition pathways were limited to the loss of an H_2 molecule or an H radical, as follows, with appearance energies calculated from RRKM theory analysis of the coincidence data.

$$C_2H_6^+ \rightarrow C_2H_4^+ + H_2 \qquad AE = 12.11eV \qquad (21)$$

$$C_2H_6^+ \rightarrow C_2H_5^+ + H^\bullet \qquad AE = 12.37eV \qquad (22)$$

The onset of other process does not appear until experiments are completed at an energy above 14.5eV. Stockbaeur[31] identifies the onset of production of $C_2H_3^+$ and $C_2H_2^+$ at approximately 14.8eV and mentions that the appearance of those ions may be related to the onset of a second

electronic state of ethane at 14.45eV. The appearance of the $C_2H_2^+$ ion arises from further H_2 loss from the ethane cation, whereas $C_2H_3^+$ could arise from the loss of H_2 from $C_2H_5^+$ or H radical loss from $C_2H_4^+$. Another product, CH_3^+ was detected in very small amounts at the maximum energy investigated in this study.

Bombach *et al.*[32] reviewed the Stockbaeur work in light of their theoretical calculations of rate and energy functions. The branching ratios for the products of ethane ionization under these PEPICO conditions are shown in Figure 2. They concluded that the loss of H and H_2 from ionized ethane is competitive, but that the reversal of the reaction that produces the $C_2H_5^+$ has no activation barrier, while the re-hydrogenation of ethane cation does, which may account for the differences in the branching ratios.

Tsuji *et al.*[33] present mass spectrometric results following charge-transfer reactions of ethane via Ar^+ and show that the major products of this reaction include $C_2H_4^+$, $C_2H_3^+$, $C_2H_2^+$, as a result of dissociative C-H bond cleavage events. In addition to these major reactions, other minor pathways include an energetically allowed C-C bond fission and some secondary reactions completed at a slightly higher flow rate. These reactions, as well as the energy remaining following the ionization pathways, are shown in Scheme 5.

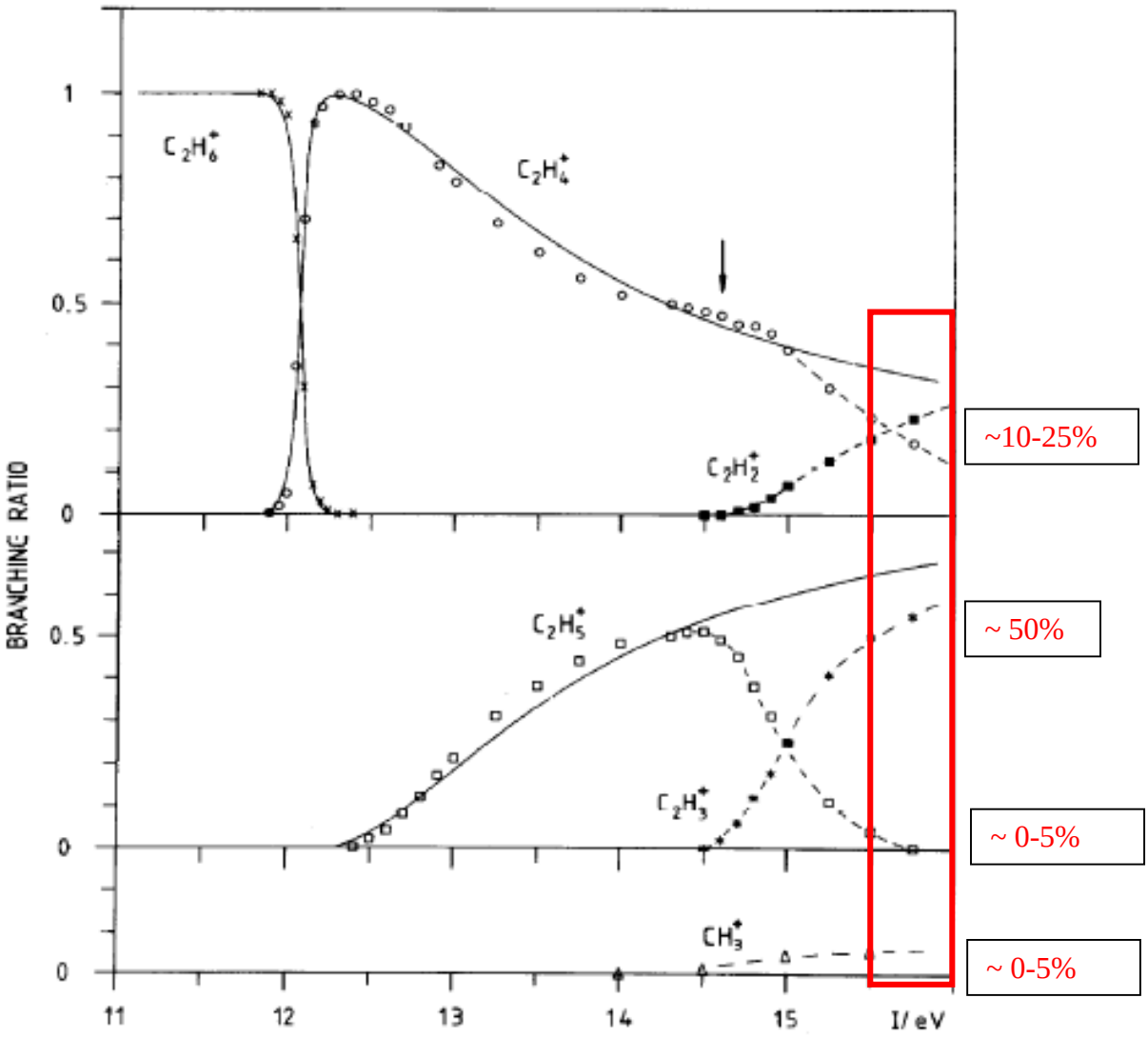

Figure 2: Branching ratios figure, adapted from Bombach *et al.*[16] to highlight the area of interest for the present work. Highlighted in red is the energy range accessed in the present work through charge-transfer with Ar^+.

Scheme 5:

Major:

$C_2H_6 + Ar^+ \rightarrow C_2H_4^+ + H_2 + Ar + 3.89\ eV$

$\rightarrow C_2H_3^+ + H_2 + H\ Ar + 1.13\ eV$

$\rightarrow C_2H_2^+ + 2H_2 + Ar + 1.29\ eV$

Minor:

$\rightarrow C_2H_5^+ + H + Ar + 3.30\ eV$

$\rightarrow CH_3^+ + CH_3 + Ar + 2.17\ eV$

The fission of the C-C bond accounts for the production of CH_3^+ and the high flow rate conditions allowing for secondary reactions accounts for the remaining product, $C_3H_5^+$, which is first observed above flow rate of 5sccm. The authors report that under low flow rates, 95% of the fragments are produced through C-H bond cleavage, whereas the minor C-C bond cleavage process accounts for only 5% of the products. The rate constants for secondary reactions that occurred under specific conditions were calculated ranging from 5.82×10^{-10} to $4.3 \times 10^{-11} cm^3 s^{-1}$. This is suggestive that the chemistry that occurs depends on the particular timescale of the experiment.

Mackie *et al.*[34] report mass spectrometry distribution data of product ions following photo-ionization of $C_2H_6^+$ by 11-40 eV radiation. The appearance energies for the $C_2H_6^+$, $C_2H_5^+$, $C_2H_4^+$, $C_2H_3^+$ and $C_2H_2^+$ ions were found to be 11.5, 12.4, 12.0, 14.8 and 14.9 eV respectively. One major difference in this study, compared to the works discussed above is that the parent ion, $C_2D_6^+$, remains and is detected in appreciable quantities. The authors discuss that the formation of the secondary process products, $C_2D_3^+$ and $C_2D_2^+$, which arise from consecutive decay

processes, depends on the statistical decay of each individual fragment ion instead of the parent ion.

Given this background research, it is generally the case that products arising following ethane ionization are characterized to a large extent by dehydrogenation events, and a lesser extent by C-C cleavage under conditions that favor unimolecular chemistry. Any other products are observed only under higher-pressure conditions that facilitate bimolecular processes, which are not of importance for the present thesis work.

The present thesis will examine the chemical processes that occur within the EBMIS apparatus following ionization of ethane at an energy of 15.8 eV. This work aims to analyze the products of ionization in order to better understand the processes that occur in these experiments in light of other work.

Chapter 3

Experimental

3.0 Overview

This section describes the specially designed systems used for gaseous sample preparation, as well as the electron bombardment matrix isolation experiments. The technical details and design rationales for each system will be covered here, as well as the protocol for general use of the apparatus. In addition, the details of the theoretical calculations used to complement the EBMIS experiments are described.

3.1 High-vacuum Pumping Systems

A successful EBMIS experiment needs to be conducted under high vacuum conditions in order to maintain the purity of the samples being studied, as well as to give the thermal insulation necessary to ensure that the cryogenic temperatures are maintained. These high-vacuum pressures are dependent on the construction and maintenance of the apparatus. Firstly, the apparatus itself is constructed with stainless steel parts in order to minimize the occurrence of outgassing. Additionally, all other connections are rated for high-vacuum to ensure that leaks do not compromise the success of the experiments by allowing atmospheric gases into the system. Finally, the low pressures are reached through the use of pumps that remove the gas particles that are introduced to the system each time a new sample is attached to the apparatus.

High vacuum pressures are obtained using a two-stage system; one that can tolerate higher pressures and begin the reduction of pressure and a second stage that reduces the pressure to the desired low pressure of $10^{-7} – 10^{-8}$ torr. During the first stage of pumping, a mechanical rotary pump (Edwards E2M2) is used to reduce the pressure inside the apparatus to

approximately $10^{-2} – 10^{-3}$ torr, which is measured using a Pirani Gauge. Following that reduction, a gate valve is opened to begin using a silicon-based diffusion pump during the second stage of pumping, which allows the system to reach high-vacuum pressures. The high vacuum pressure is out of the range of the Pirani pressure gauge, so a cold cathode ion gauge is used to give a pressure reading when the diffusion pump is being used.

During initial pumping using the mechanical pump, the gate valve isolates the diffusion pump from the rest of the system so that it does not become contaminated. The diffusion pump uses boiled silicon oil vapour to sweep away remaining gaseous molecules that come in contact with the vapour after the gate valve has been opened. The hot silicon oil is very reactive with atmospheric gases and reaction products can become a problem. If oxygen molecules are present, for example, silicon dioxide (sand) is ultimately produced, causing the pump to stop functioning properly. For that reason, the diffusion pump is used at low pressures only, when very few of these gaseous molecules are left in the apparatus.

3.2 Gas-mixture Preparation Line

Sample preparation was completed using a separate apparatus from that which is set up for the EBMIS experiment. A stainless steel, high-vacuum line is used to prepare the gaseous samples, as depicted in Figure 3. This preparatory apparatus maintains a high-vacuum pressure, using the same type of dual-stage pumping system as described in the previous section, to ensure the purity of the sample. Gaseous samples are prepared with reagents that are either already in a gaseous state, or liquid reagents where the vapour pressure can be used to collect reagent gas.

Attached to the stainless-steel preparation line are the various inlets and outlets, to allow reagents, sensors, and pumps to be attached, to ensure careful preparation of gaseous samples

that are to be used in the EBMIS experiments. As shown in Figure 3, there are several inlet tubes that are connected to the main line, in order to attach a 1-2L glass sample bulb and any other reagent container required for the particular sample preparation. Each inlet is equipped with a high-vacuum valve to either isolate the system from the atmosphere, or to allow the input of reagent gas when the valve is opened. The sample bulb, liquid reagents, or lecture bottles of pure reagent gas are fitted onto the inlet using an air-tight compression fitting to, again, ensure the highest purity of samples. There is also an inlet for the Argon gas supply, which remains permanently attached, as it is typically used as the carrier gas in the samples. Another control valve isolates the outlet that is used to pump gases out of the apparatus, through the use of the mechanical and diffusion pumping systems described earlier. The pressure of the system is monitored by a Pirani pressure gauge, as well as a cold cathode sensor to inform about when the system has reached a high-vacuum pressure.

In addition to these two pressure gauges, a digital MKS Baratron is used to accurately gauge the pressure in the system, to 10^{-1} Torr, during sample preparation. As is explained in the next section, sample preparation relies on a pressure ratio of reagent to carrier gas, and this is gauged using the Baratron. Finally, there are additional control valves placed along the preparation line, used in order to manipulate the direction of gas flow.

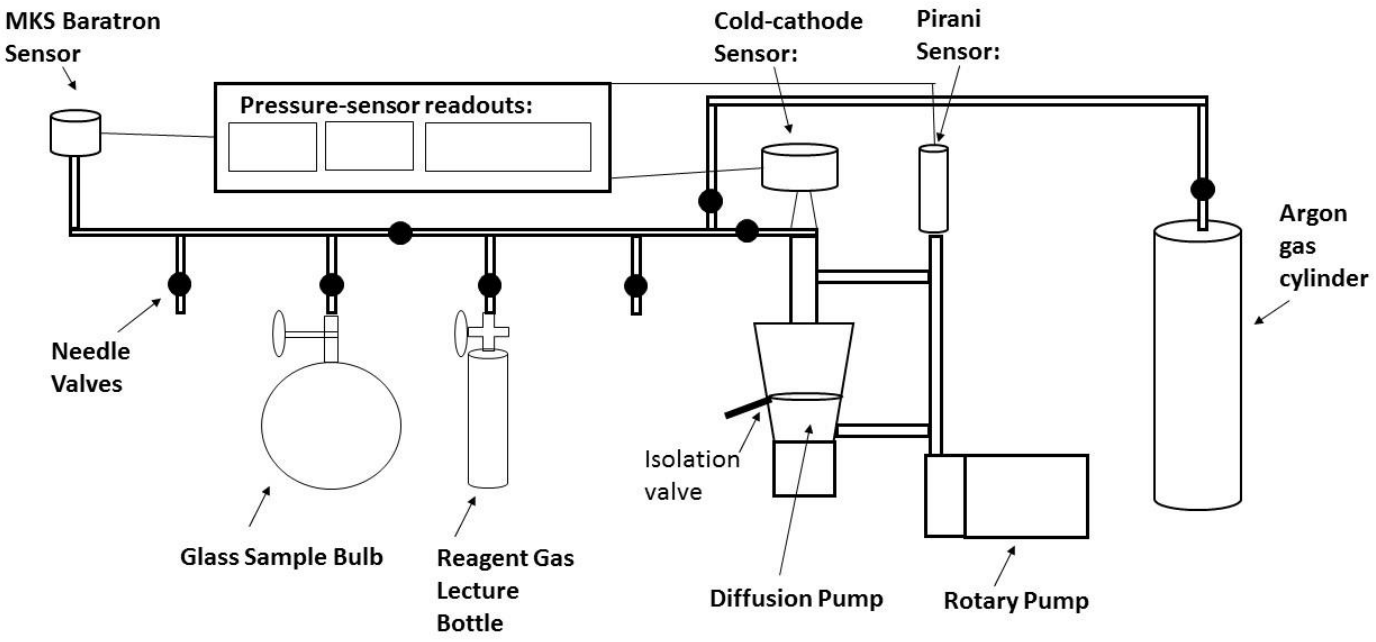

Figure 3: Vacuum-sealed gas-line apparatus for sample preparation equipped with two-stage pumping.

3.3 Protocol for Sample Preparation

Sample preparation is completed using the apparatus described in the previous section via the protocol described here. Samples are prepared in a 1- or 2-litre glass bulb, using gas cylinders of the pure reagent gas, deuterated ethane (CDN Isotopes, >99%), as well as argon (Praxair, 99.995%) carrier gas, both used without further purification. The amounts of each gas that are required to prepare a sample are dictated through a simple mole ratio calculation. The ideal gas law is used for the sample preparation calculations, but it is simplified given that the volume and temperature remain constant. This manipulation of the ideal gas law equation is shown, as follows, with an example.

$$n_a/n_b = (P_aV/RT) / (P_bV/RT) \qquad (23)$$

$$= P_a/P_b = 2.0 \text{ Torr} / 800 \text{ Torr}$$

$$= 1/400$$

Prior to sample preparation, the glass bulb is attached to one of the inlets on the preparation line, and the lecture bottle containing the deuterated ethane gas is attached to another. The system is then given time for the two-stage pumping to reduce the pressure to below 5.0×10^{-7} so that contamination is minimized. Once the bulb and all lines have been sufficiently evacuated, the reagent gas is carefully added as the first gas, since there is a lower pressure of reagent gas required, followed by the higher pressure of argon gas. The careful addition of C_2D_6 is accomplished by pressurizing a short tube that is attached between the lecture bottle and the control valve with, what equates to, a small total amount of gas. The highly-pressurized lecture bottle is then closed, and the small amount of reagent gas used to prepare the sample is added to the preparation line and sample bulb by slowly opening the control valve at the inlet to the system. Once the desired amount of reagent gas has been added, evident through

the Baratron pressure monitoring, the control valve to both the inlets are closed, trapping the gas in the glass sample bulb. The rest of the system is then pumped back down to vacuum pressures by evacuation, first using the mechanical rotary pump, and then the diffusion pump as pressures are lowered to an acceptable range for its operation. Subsequently, the argon carrier gas can then be added to the sample. Access to the pumping system is closed off using a control valve, and the preparative gas line is pressurized with the argon gas. Once the line is sufficiently pressurized, well past the pressure of reagent gas that was added, the control valve leading to the sample bulb can be opened and the argon valve opened to the extent that the pressure reading on the Baratron was continuing to increase at a good rate. These steps are completed in this important sequence to eliminate the loss of reagent gas molecules, which would have difficulty moving out of the sample bulb as long as argon gas was rushing into the bulb. When the bulb reached the desired total pressure, the control valves would again be closed and the bulb sealed off, containing the desired mole-ratio of reagent gas to carrier gas.

3.4 Components of the EBMIS Apparatus

The EBMIS apparatus used in all experiments was one constructed based on the design by Szczepanski *et al*.[35]. In general, the apparatus includes cooling and pumping steps in addition to the reaction zone into which sample gas is pumped and an electron beam is generated and directed towards, as shown in Figure 4. The high-vacuum conditions required for the experiments are reached using a two-stage pumping system using both a mechanical, rotary pump and a diffusion pump, which is essentially identical to that described in the sample preparation apparatus. Overall, the experiment consists of pumping sample gas into the reaction

chamber through a tube that is directed towards a deposition window, with or without being subjected to an electron beam, when it will condense and be held for later analysis.

The apparatus and reaction zone was isolated from the atmospheric pressure through the use of a control valve that remains closed until a sample has been connected to the apparatus. A glass bulb containing the gaseous sample was connected to the apparatus with an air-tight compression fitting in order to maintain the high-vacuum pressure conditions, achieved by the pumping system that was described earlier. Similar to that described in the sample preparation apparatus, the pressure of the system was monitored by a Pirani gauge as well as a cold-cathode sensor. A reverse helicoid pressure gauge is situated just after the shut-off control valve and before the mass-flow controller in order to measure the amount of sample gas available for experiments. An MKS 1100 series mass-flow controller was used to control the flow of gas into the reaction zone of the apparatus. This electronic flow controller is set to a desired and fixed rate, ranging from 0.1 cm^3/min to 5.0 cm^3/min. In this manner, the same amount of sample-gas can be used in each experiment. The sample gas is directed into the reaction chamber of the apparatus through a Teflon tube instead of stainless steel to avoid grounding the system which would interfere with the electron beam.

This next section of the apparatus, depicted in Figure 5, is where the reaction occurs. The gas sample is directed towards a CsI window for deposition, which is cooled by an APD Cryogenetics Displex closed-cycle helium refrigeration unit. The CsI window is held in a copper frame of an expander head which is connected to a helium compressor through a high-pressure feed cable. As described by Dunkin[36], high pressure helium is forced from the feed line into the expander head, where it expands in two stages via a rotating valve, and is recycled back out

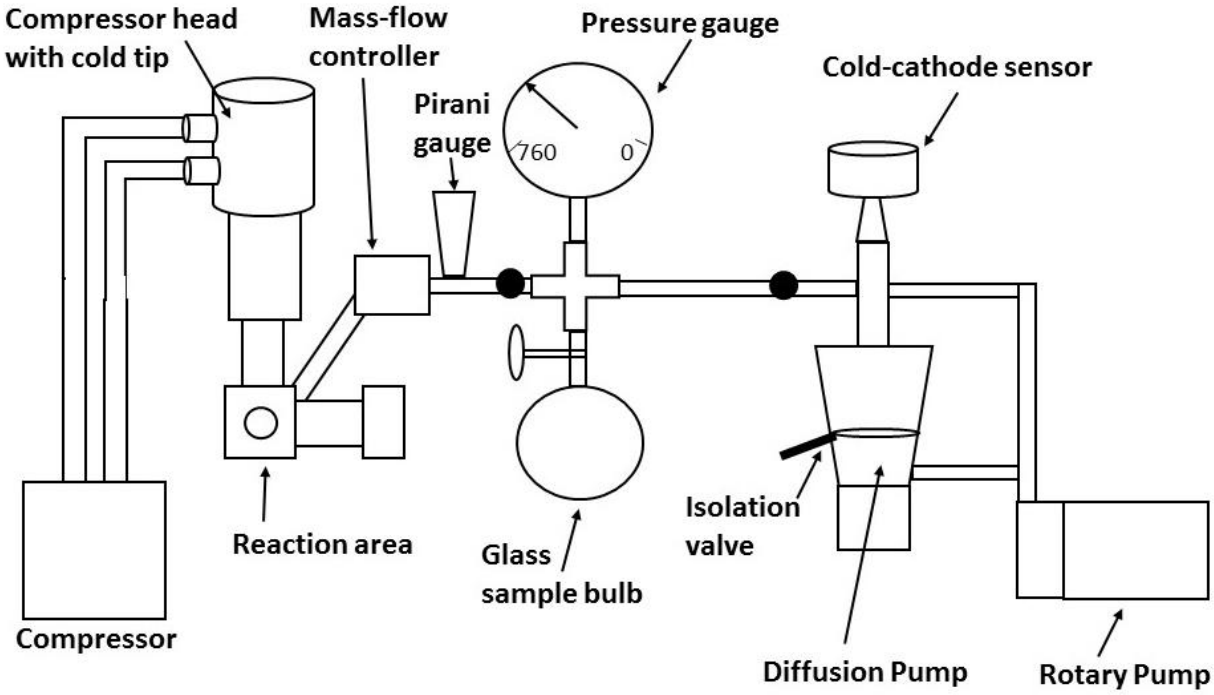

Figure 4: Schematic diagram of the EBMI apparatus, all vacuum-sealed with a two-stage pumping system. Features an inlet for a sample introduction, a reaction area where the gas sample is directed, an apparatus for achieving vacuum pressures and a compressor for cooling the deposition surface.

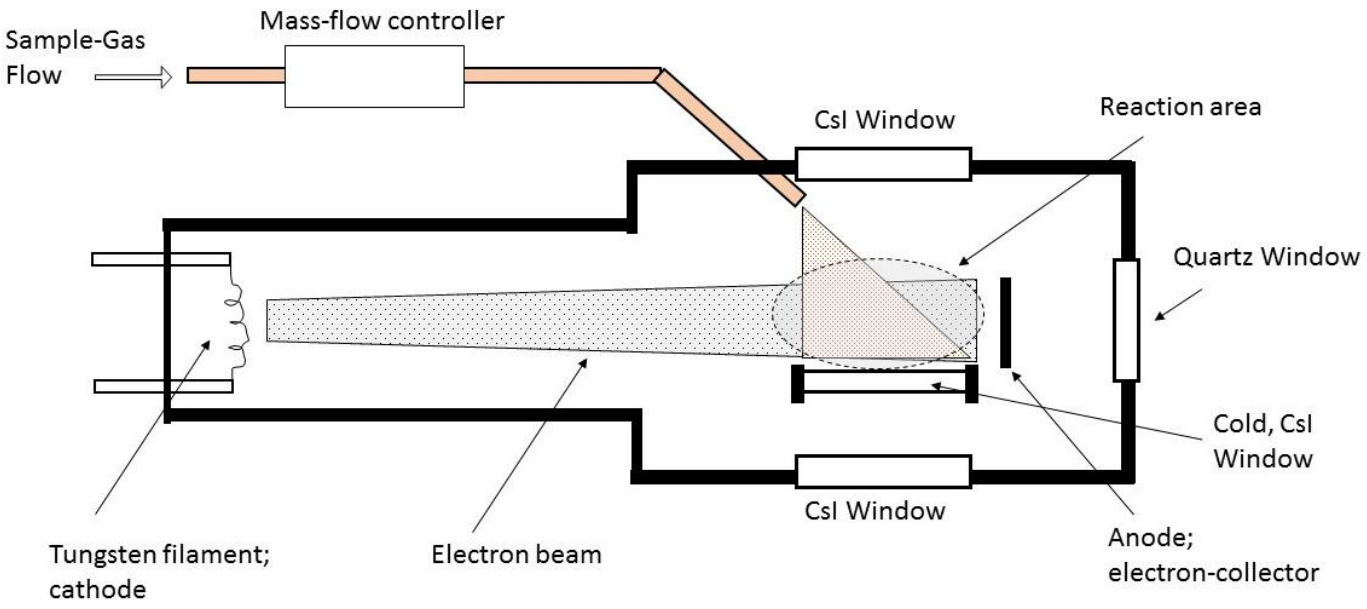

Figure 5: Schematic diagram of the reaction zone inside the EBMI apparatus, highlighting the area for deposition and positions of the anode, electron-generating filament, and the gas inlet.

through a low-pressure return cable. This movement of the helium gas results in the rapid cooling of the tip of the expander head, where the matrix deposition surface is found, through a modified Joule-Thompson effect. A temperature of about 17K can be reached after about one hour from turning on the compressor, which can maintain the cool temperature of the CsI deposition window as long as the compressor is running.

The final component of the EBMI apparatus left to describe is the generation of an electron beam that is passed through the sample gas during sample deposition in the electron bombardment experiments. A current of approximately 5.0 A was applied to a thorium-coated tungsten filament to generate electrons. The filament also acted as a cathode, with an applied voltage of -80V, in order to eject the electrons from the filament surface. An anode, located next to the CsI deposition window, was biased to ~+220V to loosely guide the ejected electrons into a beam directed as such in order to pass through the sample gas prior to reaching the window. Depending on the experiment, the anode used was either a Faraday plate (~1cm wide) or a metal pin (~1/8" in diameter), both 1.5 – 2 cm long. Given the two bias potentials, there was approximately a 300V potential difference between the cathode and anode, which helps to describe the kinetic energy of the electrons, through the following equation:

$$E_k = qV \quad (24)$$

where E_k is the kinetic energy of an electron, q is the charge of an electron, and V is the potential difference generated by the two electrodes. Given that the charge of an electron is equal to e (1.6021×10^{-19} Coulombs), and the potential difference is described in V, E_k will have units of electron volts, or eV. An eV is defined as the kinetic energy given to an electron when it is accelerated through a 1V potential difference. With a potential difference of about 300V, as is

the case for the present experiments, the electrons were generated with a kinetic energy of about 300eV, shown as follows:

$$E_k = eV = e(300V) = 300eV \quad (25)$$

The current of electrons reaching the anode was measured as a general indicator of degree of electron flux. A picoammeter, capable of reading currents from 10^{-1} nA to 2mA, was used to maintain a desired level of electron-flux by controlling the current applied to the tungsten filament. A current measured at the anode was maintained throughout each experiment, which varied from 20μA to 150μA.

3.5 Protocol for Experimental Processes

To ensure that the EBMI system was at vacuum pressures, free from contaminants, the sample gas bulb was connected to the apparatus well before the experiment was performed and allowed to pump away any small amounts of atmospheric gases that entered. Experiments were started after the series of pumps, as described earlier, brought the entire system to a pressure of 10^{-7} Torr or lower. Afterwards, the compressor was turned on to begin cooling the CsI deposition window within the expander head to approximately 17K. After cooling, which took approximately an hour to complete, a background infrared spectrum was recorded, prior to deposition of any gas, using a Bomem Michelson 100 Fourier Transform Infrared Spectrometer. Subsequently, a reference matrix of sample gas was deposited onto the CsI window for a predetermined length of time, without subjection to an electron beam. A flowmeter maintained the flow rate at 1.0 cm^3/min in order to deposit the same amount of gas in each experiment. An infrared spectrum of the reference sample gas was then collected for 100 scans at a resolution of $1cm^{-1}$, with the background spectrum subtracted from the reference spectrum. This reference

spectrum is saved and to be used later after the electron bombardment experiments to elucidate which features appear as a result of the experiment.

Prior to electron bombardment of the sample gas and deposition of the next matrix, the compressor is turned off to warm the CsI surface up to 200 K or greater in order to evaporate the gas from the reference matrix. This gas is evacuated out by the mechanical pump, the diffusion pump is used to bring the pressure back down to vacuum, and finally the compressor is turned back on to return the CsI window to 17 K. Upon cooling, the electron bombardment experiment is set up, where the anode and cathode are biased to give the 300V potential difference, as described earlier, and the 5.0A of current was applied to the filament. Following the generation of the steady electron beam, the sample gas was allowed to flow, depositing both reacted and unreacted species onto the CsI window at the same flow rate as before for the same amount of time. At the end of the predetermined time, the gas flow was stopped and another infrared spectrum was recorded.

3.6 Data Processing

The infrared data was compiled and analyzed using the computer software program Bomem GRAMS[37]. Infrared features observed in the spectra collected following an electron bombardment experiment, which were not in the corresponding experiment without electron bombardment, were considered product features. In order to compare the relative production of one species over another, the IR bands were measured through integration of the area under each peak. Wavenumber values were chosen for a particular IR band and were maintained as such for each measurement of the same product feature, for comparison between different experiments.

The measured intensities were compared relative to others of the same product and processed in a scatter plot to see the relationship of product observation against electron flux.

3.7 Theoretical Calculations

Theoretical calculations were completed for each of the vibrational modes that were used to track the production of each product of ethane ionization for the present experiments. The purpose of the calculations was to provide scaling factors to use to treat the absorption area for each measured product peak in order to correct for differences in oscillator strengths. Specifically, the calculations were a blend of Hartree-Fock, DFT (B3LYP), and MP2 methods, each using the 6-31G, 6-31G(d,p), and 6-311G(d,p) basis sets. The calculations were completed using the Gaussian 03 suite of programs[38,39]. The scaling factors were calculated by using the average predicted intensity for a particular molecular absorption band divided by the maximum predicted intensity of all molecules in consideration. By using this method, the spectroscopic absorption area measurements are converted to normalized relative concentration values, allowing for the comparison of production between products.

Chapter 4

Experimental Results

4.1 Ionization of C_2D_6 in the EBMIS apparatus

Electron bombardment (EB) experiments using a sample of gaseous C_2D_6 in Ar, with a typical mole-ratio concentration of 1:1600, were completed. This gaseous mixture was introduced to the ionization region at a flow of 1.0 cm^3/min and deposited, along with any resulting product species, onto a cold substrate window held at ~19K. Decomposition of the C_2D_6 precursor is confirmed by comparing FTIR spectra of experiments completed with EB to an experiment using the same gaseous sample without EB. Figure 6 shows a section of the FTIR spectra of two separate experiments completed both with and without electron bombardment. A marked decrease in the size of spectral features corresponding to the C_2D_6 precursor is observed in the experiment following electron bombardment. This reduction in size indicates that a portion of the precursor molecules were ionized, following electron bombardment, and converted into products.

Spectral data from the experiments with and without electron bombardment, are shown in Figure 7 for a different wavenumber range, which highlights the identified product species. Spectral features corresponding to ionization products are displayed in a difference spectrum shown by the black line in Figure 7, where the positive features correspond to vibrational modes of the products and the negative features correspond to those of the precursor.

The features displayed are the major spectral features of the matrix isolated products arising from a typical EB experiment, whereas a complete listing of the product features and their corresponding wavenumbers are listed in Table 1. Products resulting from the loss of either

a deuterium atom, $D^{\bullet}$, or molecular deuterium, D_2, seem to dominate in this system. As such, the products observed following a typical experiment include C_2D_5 (2090.6, 2051 cm^{-1}), C_2D_4 (720/22, 1074, 2201, 2345 cm^{-1}), and the products resulting from similar subsequent fragmentation of those products, C_2D_3 (703 cm^{-1}) and C_2D_2 (541, 2431/37/41 cm^{-1}). These fragmentation products of ethane have been observed in previous work completed by a group performing PEPICO experiments[34]. An additional product identified in this work, which was not predicted by the PEPICO work for the energy that we work at, is C_2D (1746 cm^{-1}). The infrared spectrum for this species has been characterized in condensed argon previously and was found to have only the one feature, corresponding to the CC stretch of the C_2D species[40]. Since these product species have already been well-characterized, the study of the ethane (or deuterated ethane) system in our apparatus will allow for the elucidation of the impact of various experimental parameters on the products observed.

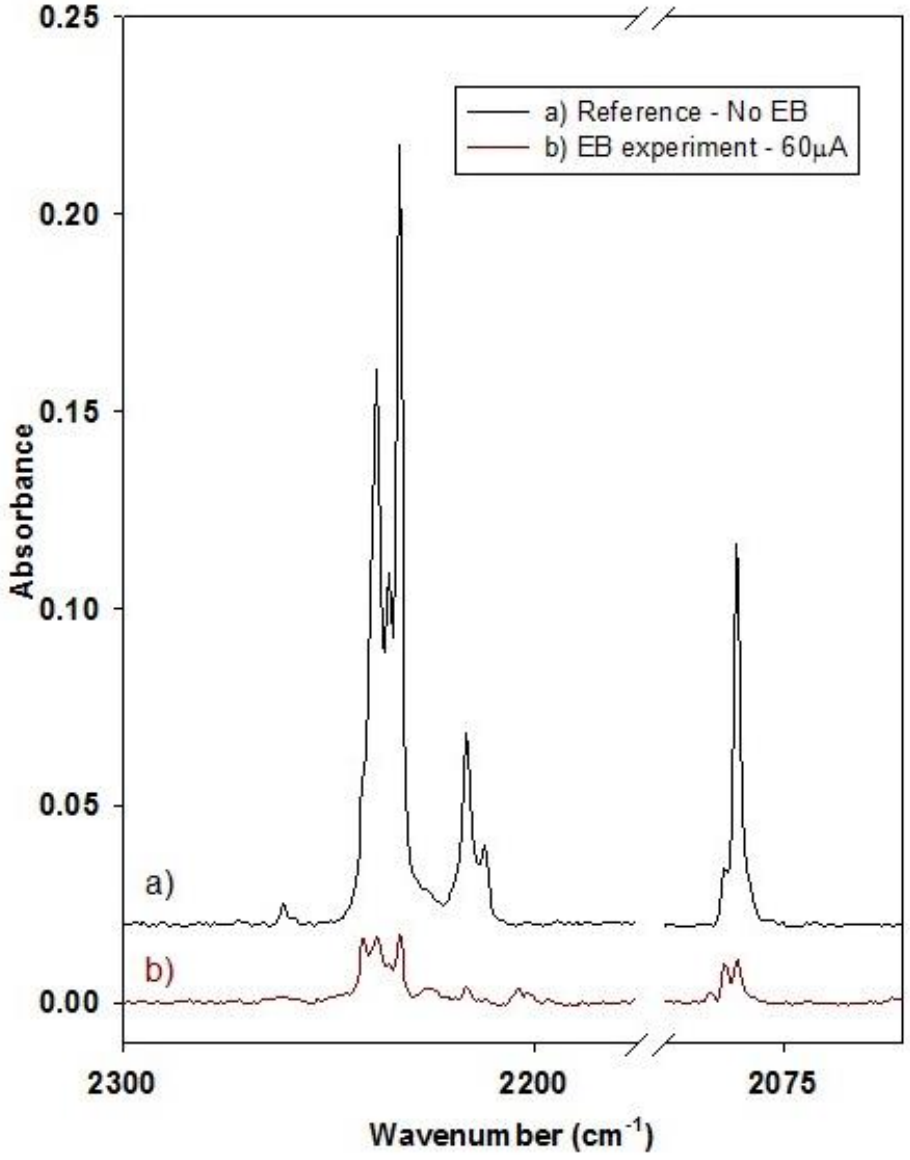

Figure 6: FTIR spectral data for a typical experiment with a 1:1600 C_2D_6:Ar sample. Shown here on the bottom, in red, is the spectrum obtained following an experiment using electron bombardment, which is compared to the spectrum on the top, in black, of an experiment of the same duration without electron bombardment. The portions displayed correspond to C-D stretching regions of C_2D_6.

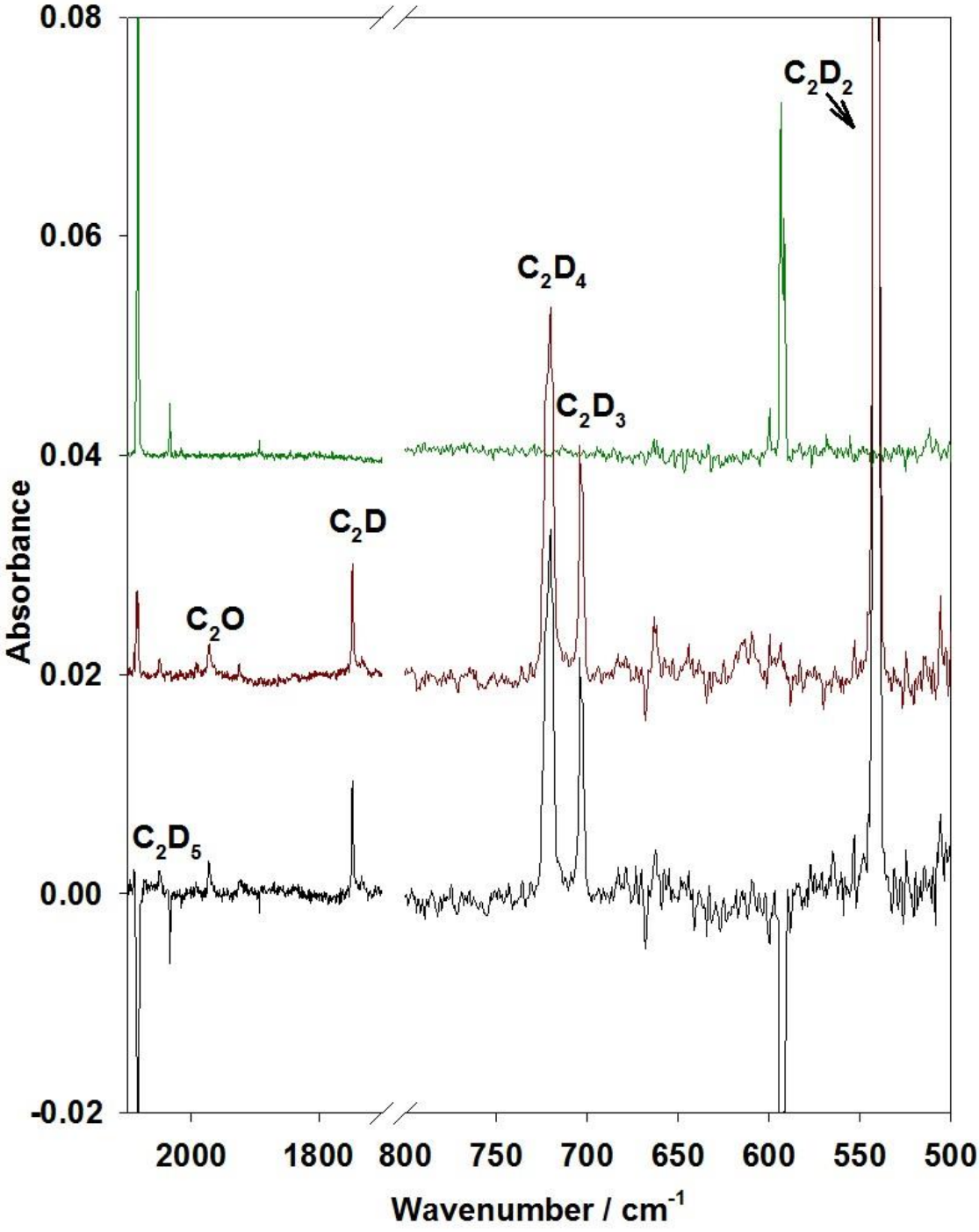

Figure 7: Portion of the FTIR spectra of a 1:1600 C_2D_6:Ar sample displayed, in black at the bottom, as a difference spectrum acquired using an electron bombardment experiment, shown in red in the middle, of 90μA ionizing electron current. Corresponding products of this are displayed as positive features whereas features of the precursor are negative. The green spectrum on the top corresponds to the reference spectrum collected without electron bombardment.

Table 1: FTIR wavenumber features associated with the matrix isolated products resulting from electron bombardment experiments with gaseous C_2D_6 in argon

Product	Wavenumber (cm^{-1})	Associated vibrational motion
C_2D_5	2090.6	CD_3 symmetric stretch
	2051	CD stretch
C_2D_4	2345	CD asymmetric stretch
	2201	CD2 asymmetric stretch
	1074	CD2 scissor
	722/720	CD2 wag
C_2D_3	703	Mixed
C_2D_2	2441/2437/2431	CD stretch
	541	CD bend
C_2D	1746	CC stretch

4.1.1 – C_2D_6/Ar: Variation of electron-flux; pin configuration

Earlier studies in our group investigated acetone ionization, the results of which indicated that the chemistry we observe upon electron bombardment changes depending on the flux of ionizing electrons. This section will be dedicated to evaluating this dependence, and investigating how the product distribution changes as a function of electron flux, using deuterated ethane, C_2D_6, as the reagent gas. Ethane was selected as the reagent because it was identified as a product of the earlier acetone decomposition work, whereas other products were identified and justified as being products of further decomposition of ethane. Using ethane as the reagent gas, directly, allows for isolation of this proposed ethane decomposition pathway, while also reducing the number of possible products observed, making it possible to more accurately describe the chemistry that results from changing the electron-flux. Samples of a reagent gas, C_2D_6, in argon with mole ratios of 1:800, 1:1600, and 1:3200 were separately studied in a series of electron-flux experiments. Changing the mole-ratio concentration of the sample was previously shown to influence the chemistry observed, because of the change in relative partial pressure of reagent gas in the ionizing region[3], and so the effect of electron-flux will be evaluated at different relative concentrations also. For each sample of C_2D_6/Ar, a series of EB experiments was completed at electron-flux currents of 150, 120, 90, 60, and 30μA, detected at the anode electron-collector.

The resulting spectra of the series of EB experiments were each compared to the reference spectrum of the experiment conducted without EB under the same experimental conditions, with the same gaseous sample. As a result of changing the electron-flux, there was an observed change in the extent of reagent decomposition. This is shown in Figure 8, where the size of spectral features corresponding to the C_2D_6 remaining, changes as the flux moves from

high to low. At relatively low electron flux, the FTIR peak that remains following an EB experiment is larger than that of high-flux experiments, indicating that less of the reagent has been converted to product. This indicates that the fraction of decomposed C_2D_6 increases with electron flux, however, as shown in Figure 9, it does not follow a linear trend. Figure 9 also shows how the extent of C_2D_6 decomposition changes with electron flux for samples with differing mole-ratio concentrations as listed above (1:800, 1:1600, and 1:3200). It is apparent that a greater fraction of C_2D_6 is consumed and converted to products for samples with a low mole-ratio concentration of reagent gas compared to those with relatively higher concentrations. The amount of destruction at the lowest current varied from 33% for the 1:800 sample, to 68% and 63% for 1:1600 and 1:3200 respectively. For the greatest current studied, 150μA, the amount of precursor destroyed increased to 79% for the 1:800 and to almost complete destruction for the 1:1600 and 1:3200 samples, at 93% and 98% respectively.

The main spectral features of the previously listed products resulting from ionization of C_2D_6 in our EBMI apparatus are plotted for each electron-flux experiment to roughly compare the yield of a particular product to the electron-flux parameter of our experiments. The bending modes of C_2D_4 ($720cm^{-1}$) and C_2D_3 ($703cm^{-1}$) products are shown in Figure 10 for each of the EB experiments in the series. It is apparent that in the case of C_2D_3, the yield increases with electron-flux, whereas the yield of C_2D_4 is greatest at low electron-flux currents and decreases in the higher-flux experiments. Displayed in Figure 11 is the production of C_2D_2 ($541cm^{-1}$) in these experiments, which generally increases with electron-flux as did the C_2D_3 product. The C_2D_5 product is shown in Figure 12, where small features at 2090 and $2051cm^{-1}$ are observed and follow a general decreasing trend with electron-flux, similar to C_2D_4. Figure 12 also shows the

yield of C_2D (1746cm^{-1}) over the set of experiments, where a maximum yield occurs in the experiment with the greatest flux of ionizing electrons.

These product yield trends are shown in Figure 13 where peak integrations for each product are normalized within each product set with respect to the highest value for a particular product feature, and plotted against electron flux to show the relative yields and where the maxima occur. The yield of both C_2D_5 and C_2D_4 maximize at the low currents and then decrease in yield as current is increased. The changes in the yields of C_2D_3 and C_2D_2 are not as drastic, but appear to maximize in the middle of the range of currents studied and begin to taper off as electron-flux increases further. The highly dehydrogenated C_2D product is observed minimally at low currents and maximizes at the highest current. Overall, it can be seen from these figures that the relative yield of individual products changes with electron current. It is thought that these dehydrogenated species could be a result of subsequent ionization of primary products, as discussed below.

To fully analyze the data from these experiments with the pin-type anode, the same integration data for the products of C_2D_6 ionization were corrected for the oscillator strengths of each vibrational mode. By normalizing the strengths of vibrational oscillation of each of the product features, one can more-directly compare yield of products. These manipulated data are displayed in Figure 14 at the end of this section.

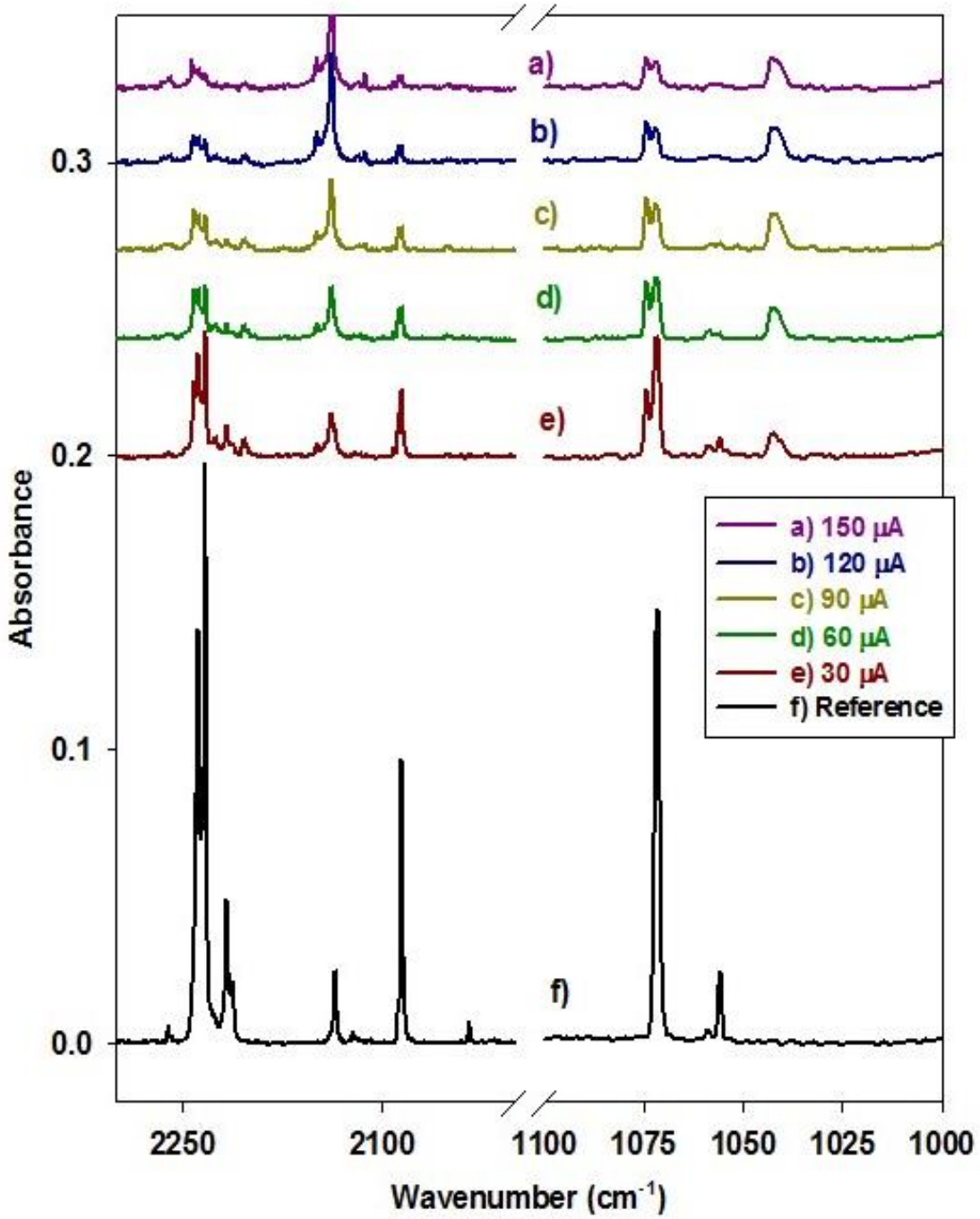

Figure 8: Spectral data of electron bombardment experiments of various relative flux compared to a reference, collected without electron bombardment. Samples were prepared with a 1:1600 C_2D_6:Ar mole concentration and experiments were completed using the pin-type anode and a flow rate of 1sccm for 2 hours.

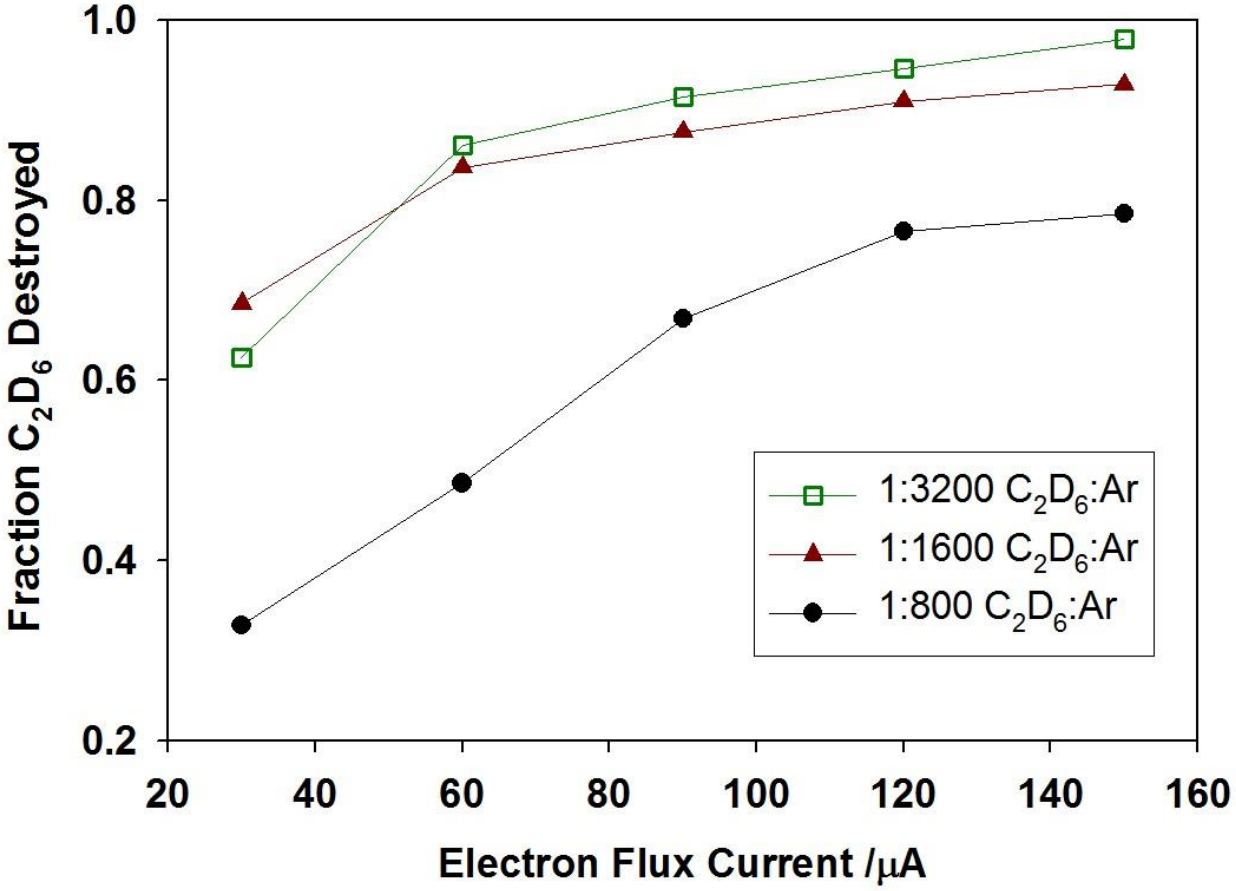

Figure 9: Fraction of reagent destroyed following electron bombardment of varying flux for sample of three different mole concentrations.

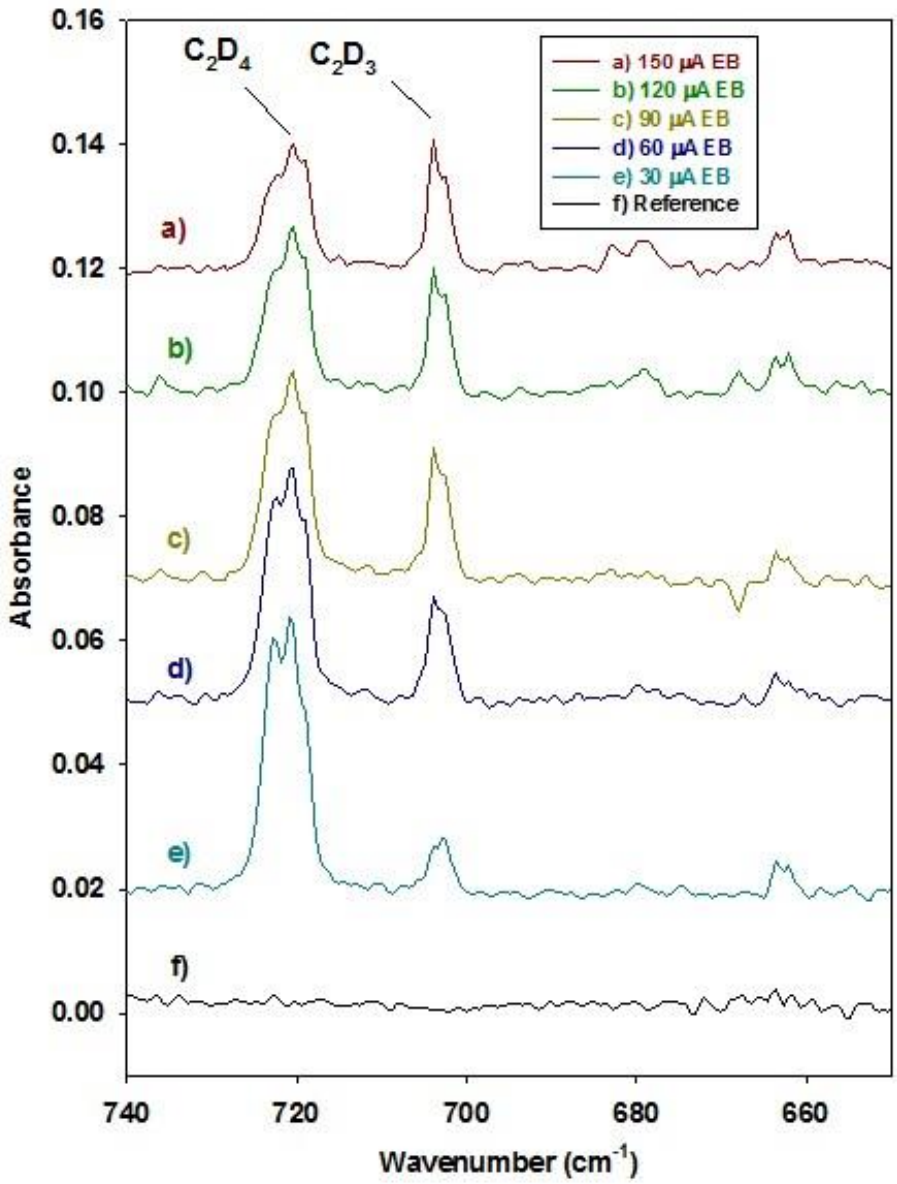

Figure 10: FTIR spectral features of two products of C_2D_6 ionization in the EBMI system, C_2D_4 and C_2D_3, at 720 and 703 cm^{-1}, respectively. Shown here are five experiments with electron bombardment, at different electron flux conditions, and one reference.

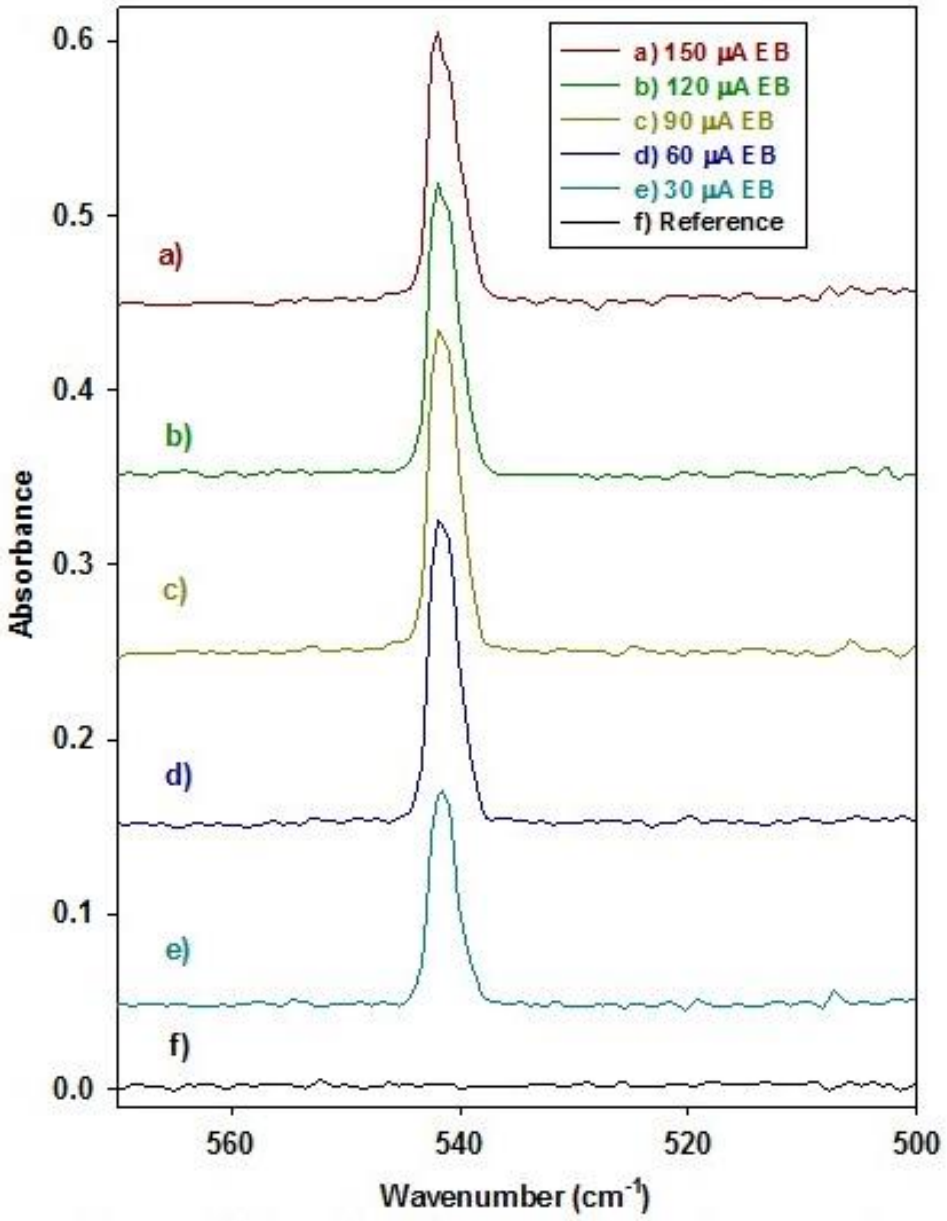

Figure 11: FTIR spectral features of the C_2D_2 product at 541 cm^{-1} following ionization in the EBMI system using the pin anode. Shown here are five experiments with electron bombardment, at different electron flux conditions, and one reference.

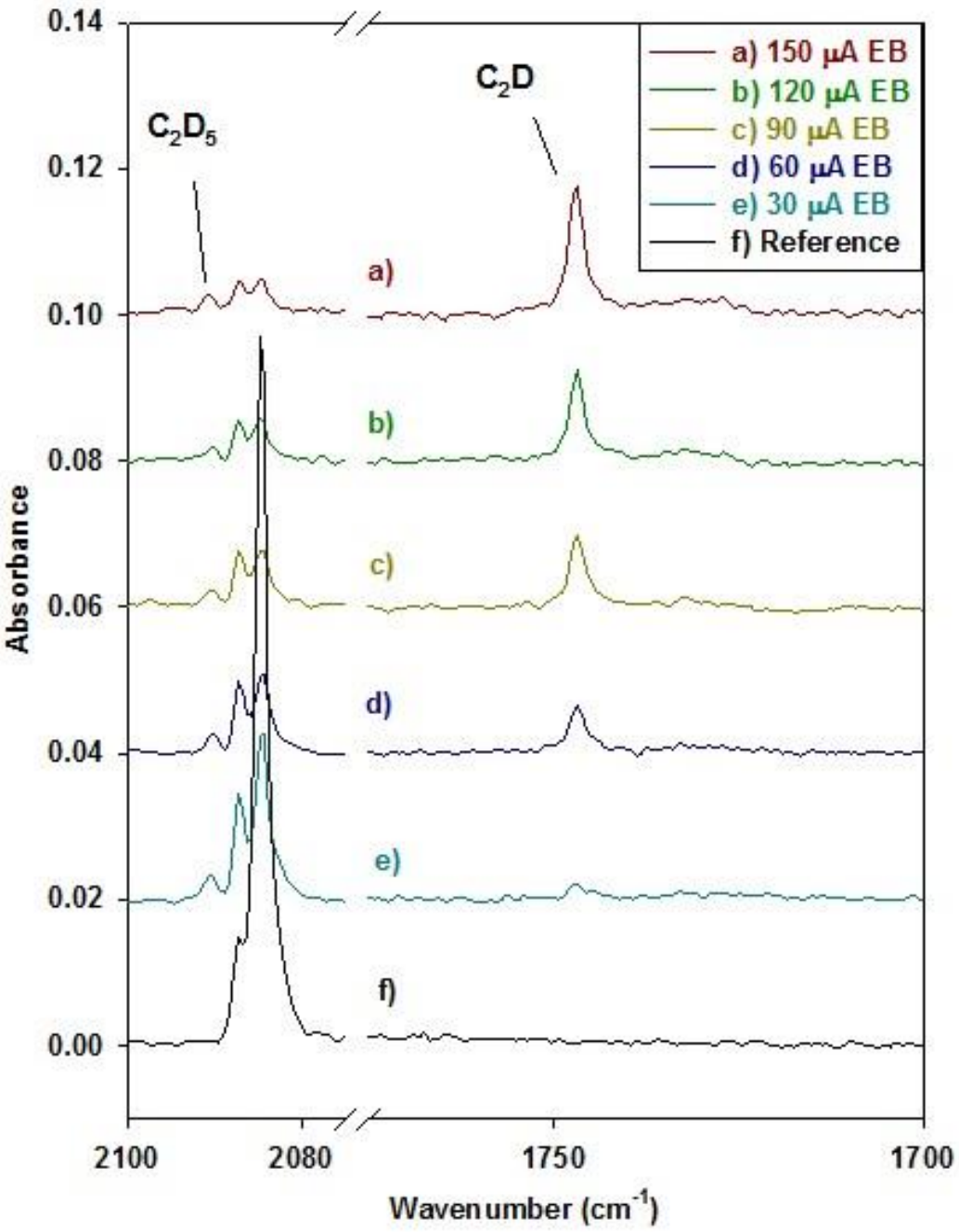

Figure 12: FTIR spectral features of the C_2D product at 1746 cm^{-1} as well as the $C_2D_5^+$ at 2092 cm^{-1} following ionization in the EBMI system using the pin anode. Shown here are five experiments with electron bombardment, at different electron flux conditions, and one reference.

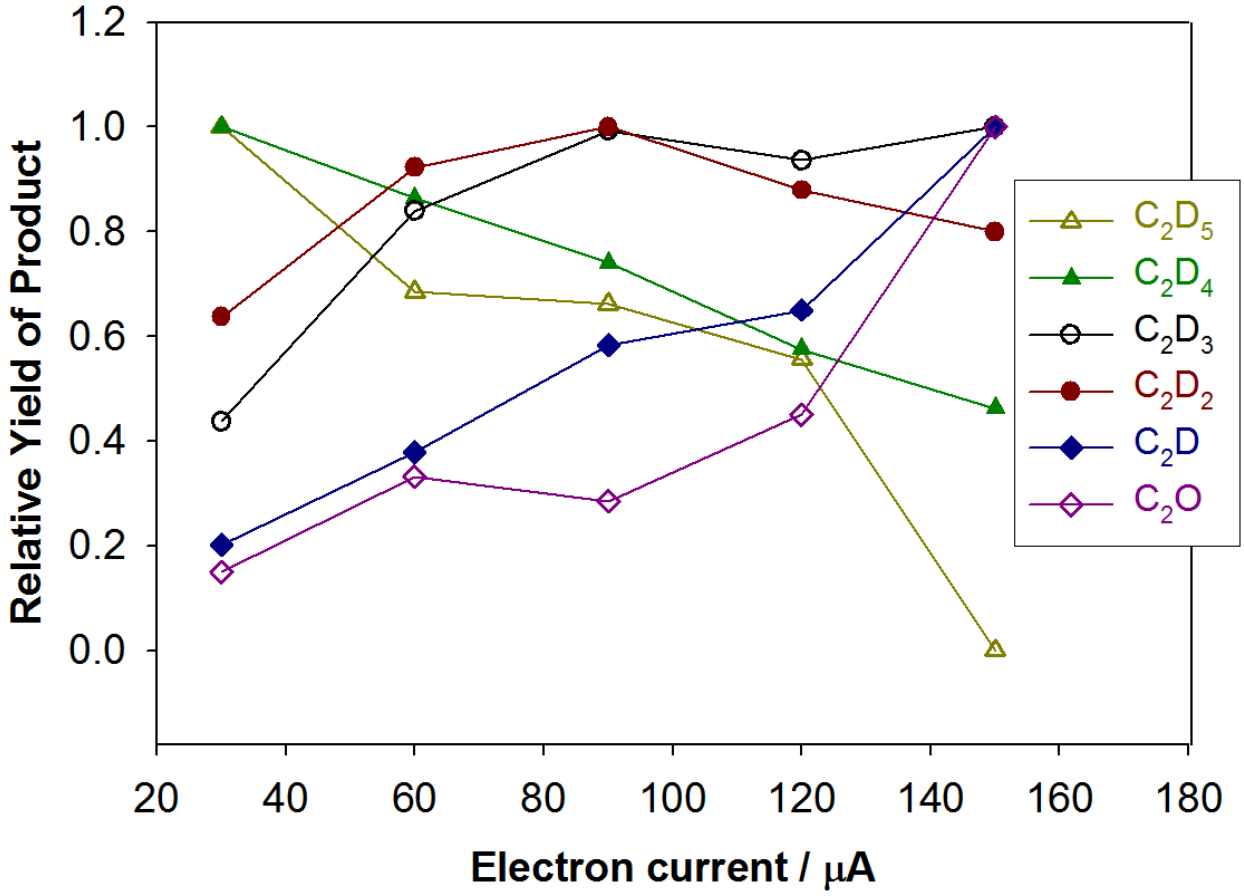

Figure 13: Product distributions for experiments completed under a range of electron-flux conditions from 30-150 μA. Products are plotted as a relative yield, normalized within each individual set of data for a specific species.

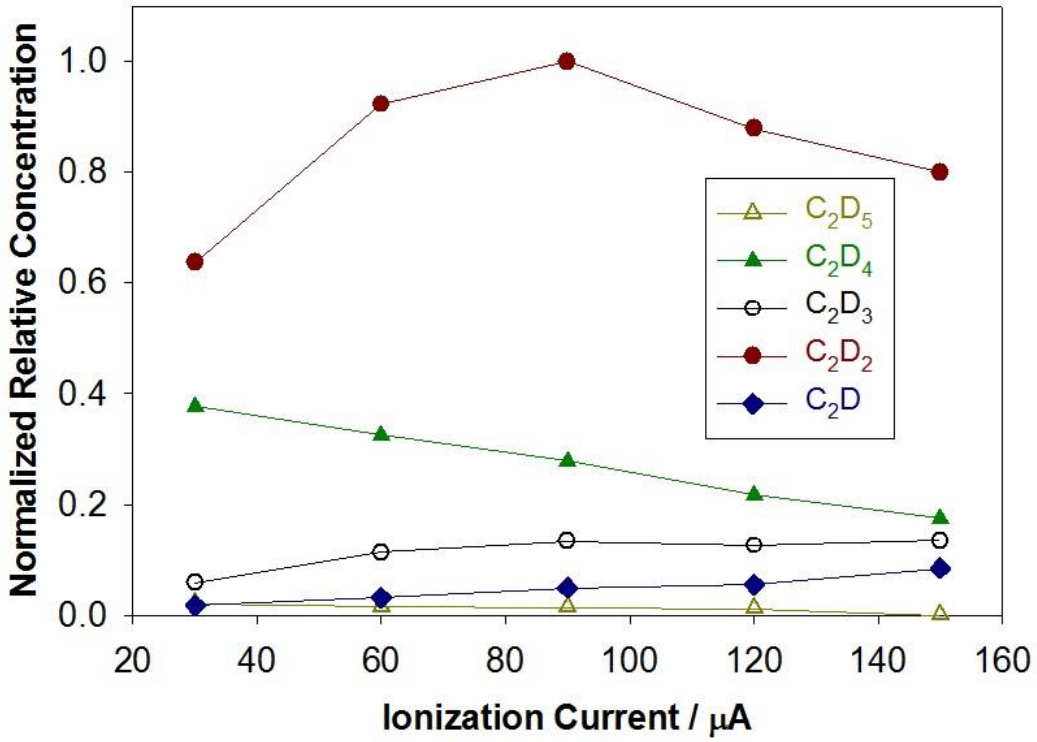

Figure 14: Product distributions, each corrected for the differing vibrational oscillator strengths for the spectral features used for integration. Experiments completed under a range of electron-flux conditions from 30-150 μA. Products are plotted as a relative yield, normalized within each individual set of data for a specific species after applying the correction factor.

4.2 – C_2D_6/Ar: Modification of anode size; plate

Given that the highly dehydrogenated C_2D product is present even under low electron-flux conditions, it was apparent that with the current experimental set-up, secondary ionization processes could not be avoided. As such, a modification to the apparatus was proposed, where the anode was made into a plate-like structure, rather than a pin as in the original set-up, in order to try to lower the electron density in the ionization region in an attempt to minimize subsequent ionization of primary products. By increasing the size of the anode, which acts as an electron collector, the electron field in the ionization zone weakens. This change was hoped to increase the dispersion of the electron beam and have an effect on the products observed.

Successful decomposition of the C_2D_6 precursor with this new anode configuration is confirmed by the reduction in the C_2D_6 peak in the spectrum following EB compared to that in the reference experiment without EB, as shown in Figure 15. The destruction at this particular current, 90μA, was calculated to be approximately 35% of the total C_2D_6 used in the experiment.

The observed products of these experiments with the plate-like anode were reduced to only C_2D_4 and C_2D_2, as shown in the spectral figure of a typical EB experiment in Figure 16 with features corresponding to those previously mentioned. Some of the product features that were previously identified upon electron bombardment of C_2D_6 in our apparatus were absent from the EB spectra after the modification to the anode, including C_2D_5, C_2D_3, and C_2D. Figure 16 shows the absence of the features that would be observed if these products were present, as in the experiments with the pin-like anode. This change in observed products indicates that the ionization events have change significantly as a result of the modification.

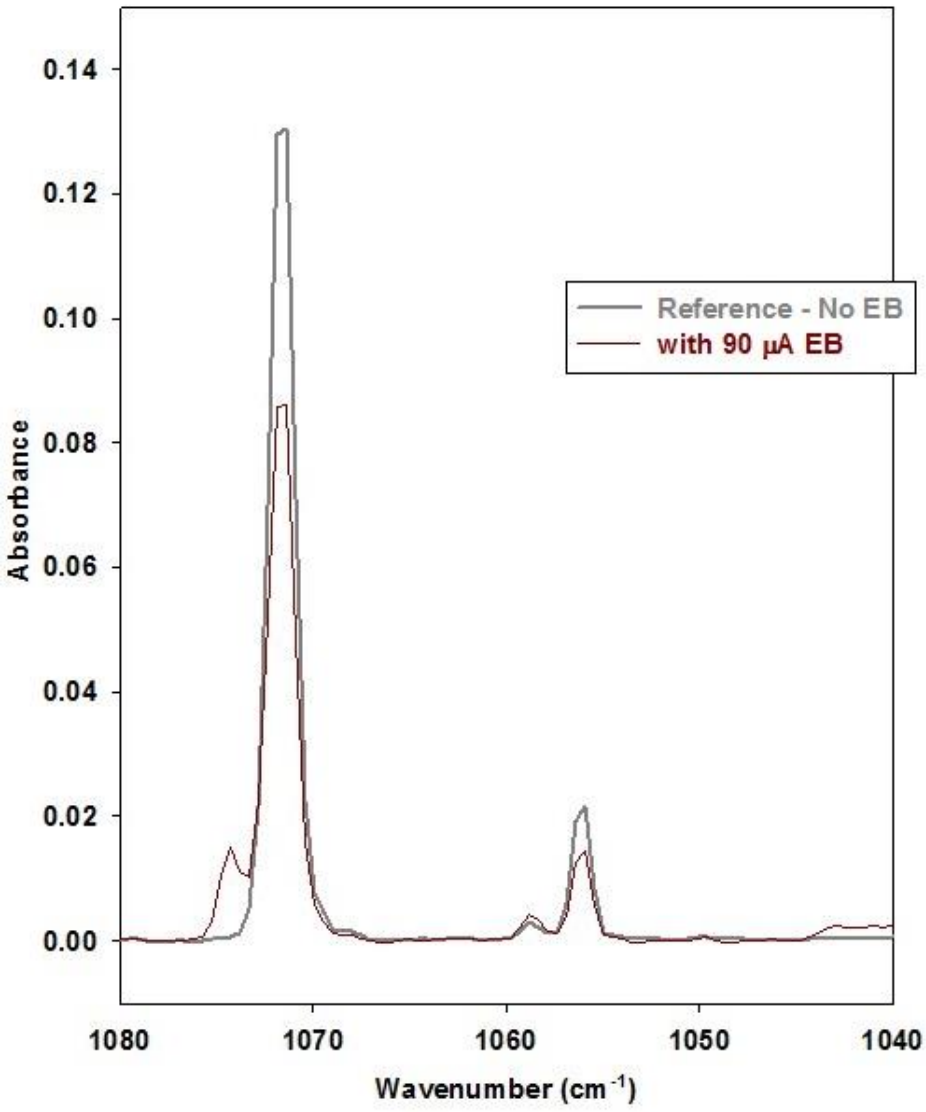

Figure 15: FTIR spectral data for experiments completed both with and without electron bombardment, using the plate-type anode. Features shown that are observed in both spectra represent features relating to the precursor and show successful decomposition of a portion of the 1:1600 mole concentration reagent sample.

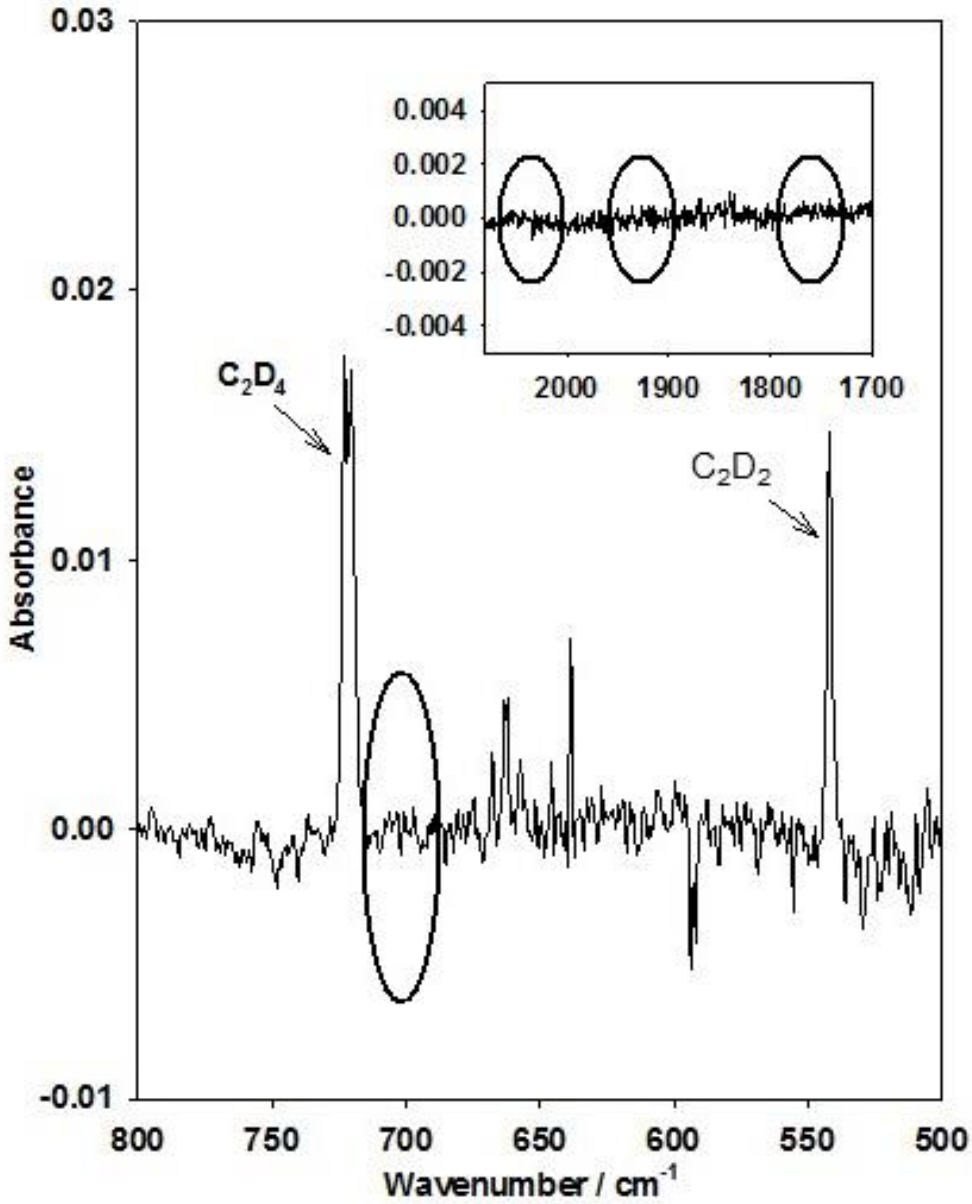

Figure 16: Spectral data from 60 μA experiments completed with the plate-type anode and a 1:1600 C_2D_6:Ar sample. A portion of the difference spectrum of this experiment is shown here, where the reference spectrum is subtracted from the experiment with electron bombardment. Displayed are features of the two sole products, C_2D_4 and C_2D_2, with ovals indicating where features would have been if C_2D_5, C_2D_3, and C_2D had been observed as in pin-anode experiments.

4.2.1 – C_2D_6/Ar: Variation of electron-flux; plate

The influence of electron-flux on the experiments with C_2D_6/Ar was studied using this newly configured apparatus with the plate-type anode. Experiments were completed using a C_2D_6/Ar mole-ratio concentration of 1:1600 over a range of electron-flux conditions, averaging at 20, 30, 40, 50, 60, 70, 80, and 90μA currents. Figure 17 shows that the extent of C_2D_6 consumption changes as electron flux is varied in a similar spectral plot of a major feature for each separate experiment. It was calculated that at the lowest current studied, 20μA, there was approximately 5% destruction, whereas the destruction reached about 30% for the experiment when the current averaged 90μA. The percentage of precursor destroyed as electron current is varied is shown in Figure 18 and, generally, shows a linearly increasing trend, albeit much lower percent destruction than in previous experiments at this current with the pin-type anode.

The yield of both major products, C_2D_4 and C_2D_2, changes with electron flux as well, shown in Figure 19, where the change in the size of the spectral features corresponding to these products are displayed. For both products there is an overall increase in the yield as the electron-flux parameter of the experiments is increased. In Figure 20, the integration of the corresponding infrared features for both C_2D_4 and C_2D_2 is shown, upon normalization within the product set, and plotted against electron flux, to show this trend.

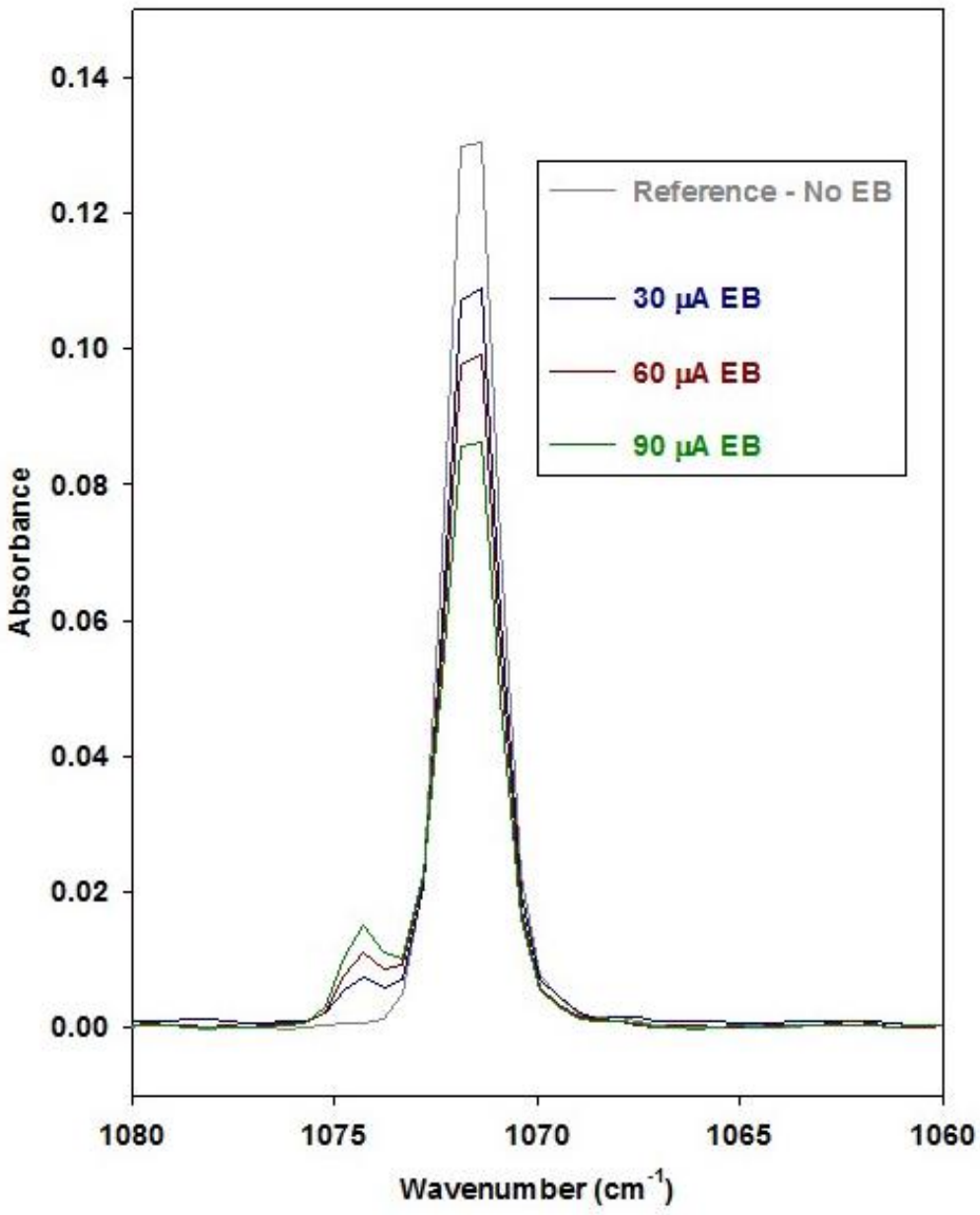

Figure 17: Shown here is a major infrared absorption feature for C_2D_6 for an experiment completed with no electron bombardment, and three others with electron bombardment of differing flux. All experiments were completed using the plate-type anode.

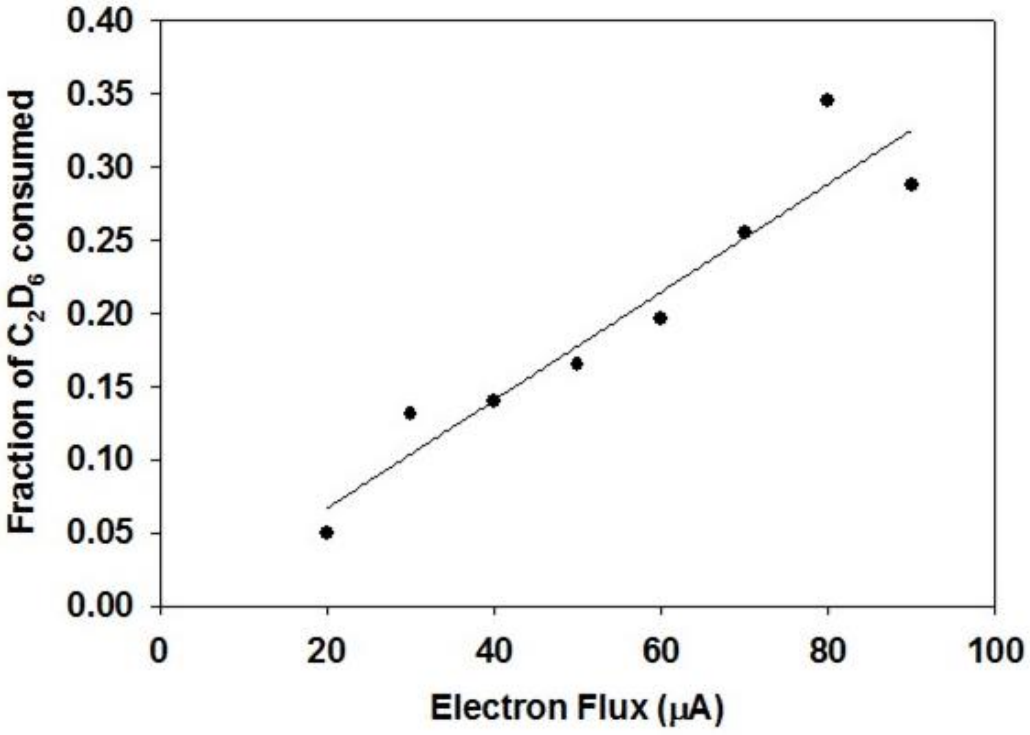

Figure 18: Shown here are the changes in the fraction of C_2D_6 destroyed for experiments of differing electron flux, using the plate-type anode. Included is a line to guide the eye to the trend of increased consumption as a function of electron flux. The uncertainty in the data is ± 5% in both the horizontal and vertical measurement.

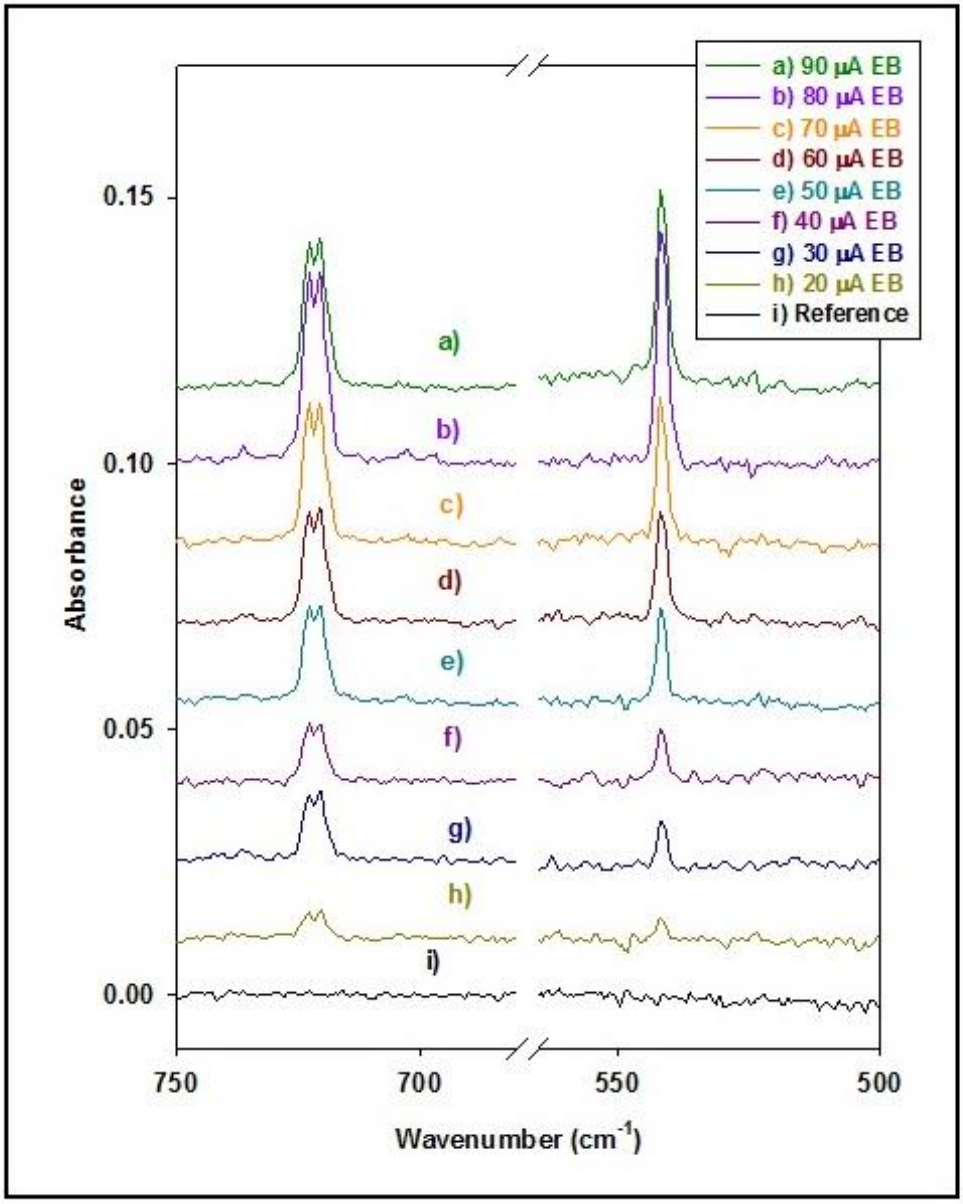

Figure 19: Displayed here is the spectral data for each of the experiments completed using the plate-type anode, showing that the yield changes with electron-flux. The feature at 541 cm^{-1} corresponds to the C_2D_2 product, whereas the feature at 722/20 cm^{-1} corresponds to C_2D_4.

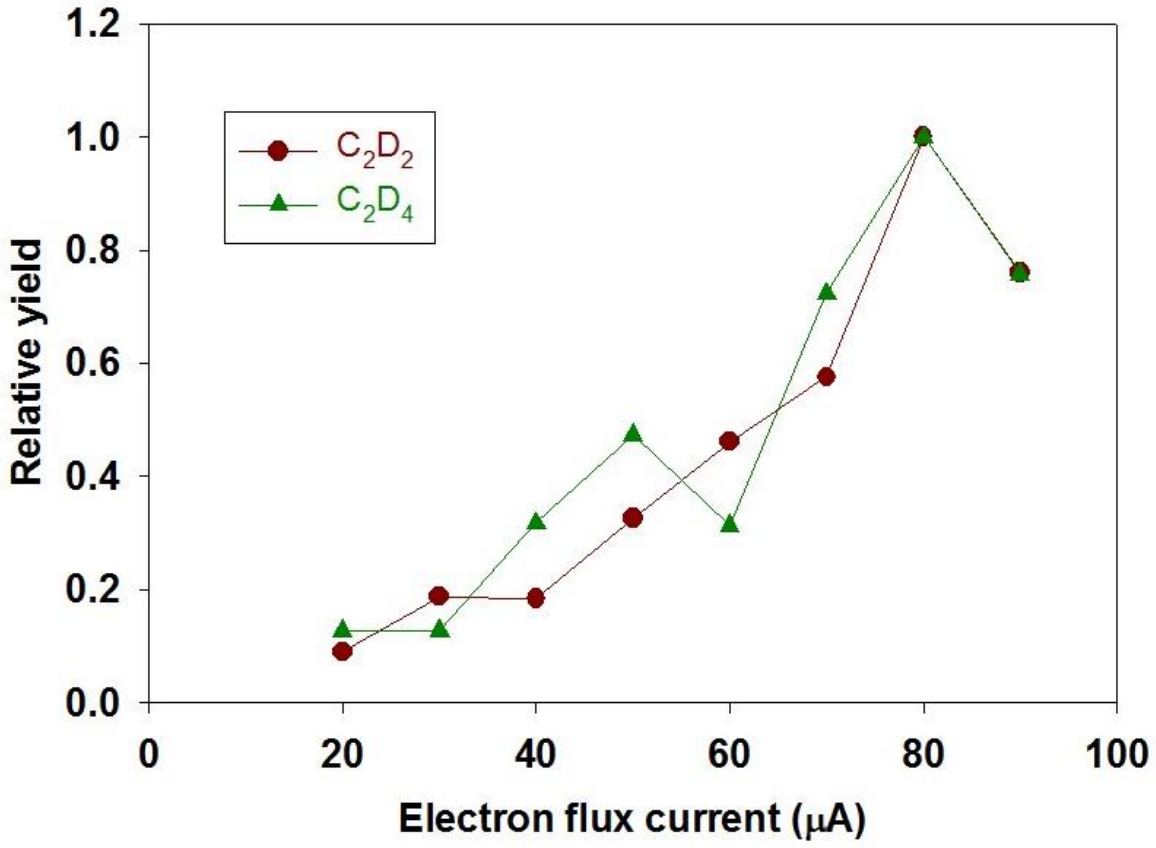

Figure 20: Product yields of the sole two products, C_2D_4 and C_2D_2, following electron bombardment of a 1:1600 C_2D_6:Ar sample completed using different electron-flux conditions. Yields are corrected for differences in oscillator strengths, and normalized, here, with respect to the greatest yield for each product.

Chapter 5

Discussion

5.0 Overview of products, in general.

The results presented in Chapter 4 will be discussed here to explain the types of reactions that occur in the EBMIS apparatus following ionization. Overall, the results clearly show that the products of ionization of gas-phase deuterated ethane diluted in argon vary, depending on the experimental conditions used. In general, the products observed are a series of increasingly dehydrogenated forms of the initial ethane molecule. The decomposition of ethane has been studied numerous times in the past where the products are mostly in accord with the current work. Products of ethane ionization, including $C_2D_5^+$, $C_2D_4^+$, $C_2D_3^+$, and $C_2D_2^+$, have been observed in the past work by Stockbaeur *et al.*[31], Bombach *et al.*[32], Mackie *et al.*[34], and Tsuji *et al.*[33]. The details of those past studies are reviewed in Chapter 2, and put into context with the present work in this discussion section. An important difference in the present experiments in comparison to the previous work, is the observation of C_2D following ionization during select experiments. The implications of observing this product will be discussed in a later section, below.

In order to discuss the possible reaction mechanisms of the work in this thesis, it is important to revisit the reason that the products of a typical EBMIS experiment are neutral. It is generally accepted that neutralization of products occurs within the condensed matrix because of the presence of low-energy electrons that are mobile in the matrix. The production of neutral products as a result of fragmentation of excited neutral ethane molecules is not considered as a valid reaction pathway within the EBMIS apparatus. Other works show that hot neutral ethane undergoes C-C cleavage to produce $CD_3^{\cdot}$[41] as a major reaction pathway, however, the absence of

this product in the present work demonstrates that products do not arise from excited neutrals in the EBMIS apparatus. The present work is consistent with the products arising from neutralization steps following initial ionization of the ethane molecule.

The chemistry observed in the present study changes depending on the specific experimental conditions, and so a full mechanistic understanding requires consideration of the processes available under the various ionization conditions of the experiment. Analysis is simplified by considering the ionization products observed under the low ion density experiments first.

5.1 Low ion-density conditions:

It is expected that ionization of ethane molecules in the reaction region is done through charge transfer (CT) ionization reactions with Ar^+. This type of ionization would leave the recipient ethane with a corresponding maximum internal energy of 4.3eV, given that 11.5eV are initially used to ionize ethane. The results show that ionization of C_2D_6 using the EBMIS apparatus, along with experimental parameters that produce low ion-density conditions, produce two major dehydrogenation products: C_2D_4 and C_2D_2. As observed in Figures 19 and 20 in the results, these are produced in significant quantities, with minimal standard deviation, at a ratio of (1.4 ± 0.1):1 (C_2D_4:C_2D_2). This product distribution loosely corresponds with other published research of ionized ethane molecules at the same energy as the present experiments, 15.8eV.

This ratio of approximately 1.4:1 ethene:acetylene most closely resembles the results of Mackie *et al.*[34] following photoionization and immediate detection by quadrupole mass spectrometry. Mackie *et al.*[34] also observe significant quantities of $C_2D_5^+$ and $C_2D_3^+$ as products, which are not observed in the present work under low ion-density experimental conditions. The

absence of these two products can be explained in terms of the neutralization events that occur uniquely in the matrix isolation experiment. The reported ion distribution by Mackie *et al.*[34] gives ion distributions of about 60% $C_2H_4^+$, 10-12% each of $C_2H_6^+$, $C_2H_5^+$, $C_2H_3^+$, and 5% of $C_2H_2^+$. These distributions are displayed below in Figure 21, reproduced from Mackie *et al*[34], for clarification. In the present work, it is appropriate to consider that the $C_2D_5^+$and $C_2D_3^+$ are observed as C_2D_4 and C_2D_2 following neutralization. Adapting from Figure 21, and considering that the 10-12% each of $C_2D_5^+$ and $C_2D_3^+$ products would be added to the original 60% $C_2D_4^+$ and 5% $C_2D_2^+$ products, the approximate observed branching ratio of these two products should be close to 4.7:1 C_2D_4:C_2D_2. Since the actual observed ratio from the present work is smaller, at 1.4:1, further decomposition of some kind must be occurring.

Further partial cation decomposition may occur prior to neutral-stabilization in the matrix. Other work have reported contrasting results to the work by Mackie *et al.*, in which the branching ratio of ethene:acetylene production is somewhat reversed. These experiments by Tsuji *et al.*[33] and Bombach *et al.*[32] also both indicate that we should expect $C_2D_3^+$ to be the primary product of our experiments if charge-transfer were the only process to consider for our experimental conditions. The $C_2D_3^+$ product, however, is not the primary product in the low ion-density potion of the present work, but instead, the two major products are $C_2D_4^+$ and $C_2D_2^+$. Based on branching ratios reported in the PEPICO[32] and SIFT[33] (Selected Ion Flow Tube Mass Spectrometry) work completed at an energy similar to the present thesis work, a ratio of 1:2 C_2D_4:C_2D_2 should be expected. This ratio takes into account that, in the present work, $C_2D_5^+$ and $C_2D_3^+$ products are expected to undergo H^+ loss during the neutralization process.

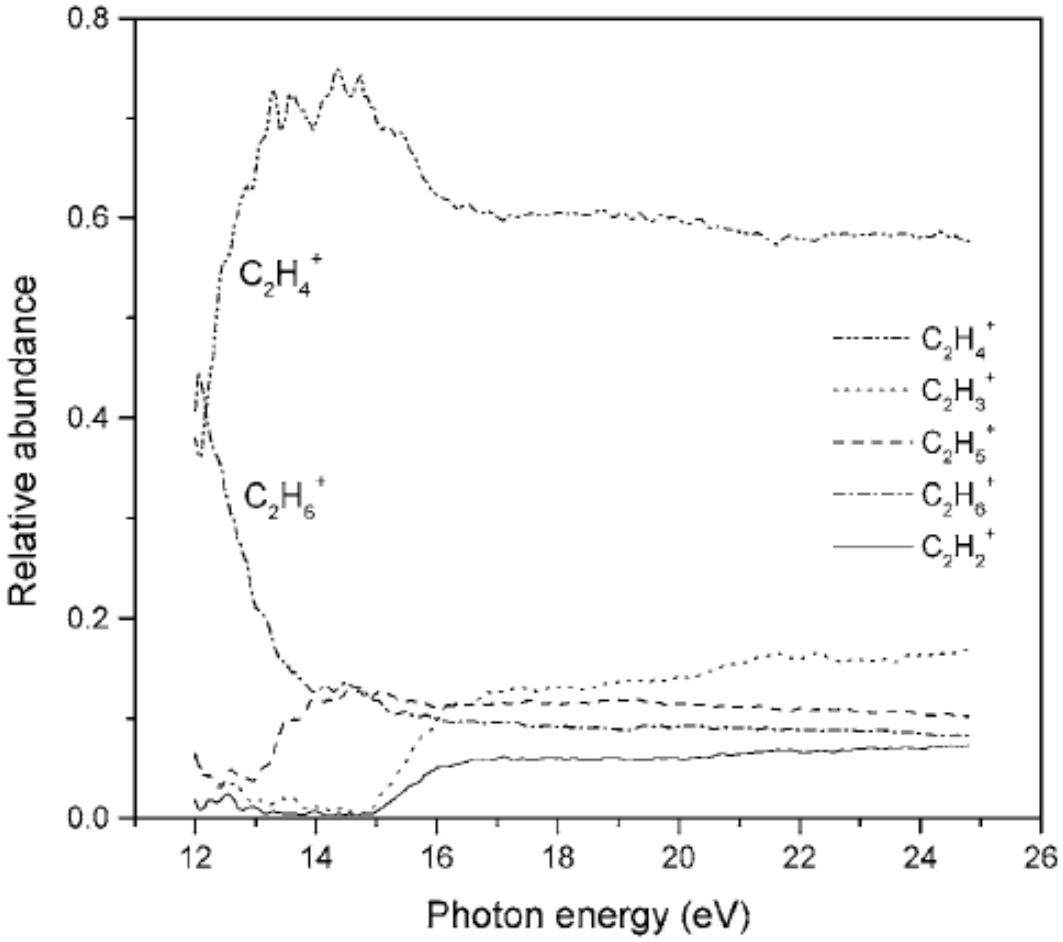

Figure 21: Reproduction of data from work by Mackie *et al.*[3] displaying the product ratios detected through quadrupole mass spectrometry, following photoionization of ethane.

The disparity between the expected ratios in each of these works can be explained based on differences in the experimental conditions. Primarily, there are differences in the timescales of detection following ionization of the past work with CT ionization of ethane, and the present EBMIS experiments. The detection of the parent ion, $C_2H_6^+$, in the Mackie *et al.*[34] experiments indicates that detection occurs significantly faster than in other work where the parent ion is not detected. The works where there is an absence of $C_2D_6^+$ detection, indicates that the ions have had the time to undergo complete degradation of precursor[31,32,33]. The extended timescale prior to detection can also explain the increased amounts of $C_2H_2^+$ via partial degradation of the $C_2H_4^+$ product ion. Given that our reported product ratio is between that of Mackie *et al.*[34], and the three studies by Tsuji *et al.*[33], Stockbauer *et al.*[31], and Bombach *et al*.[32], an intermediate timescale for experiments in the present work is implied.

Evidence that the timescale of the present work is between that of the PEPICO and SIFT work and that of Mackie *et al.*[34] is given by the intermediate product ratio calculation and by the presence of precursor molecule after ionization. There is less decomposition of the precursor expected in our experiments as compared to the earlier PEPICO and SIFT work, but increased decomposition as compared to the Mackie *et al.*[34] experiments. Figure 22 below illustrates the approximate timescales of the various experiments discussed and gives an estimation of how our experiments from the EBMIS apparatus compare in terms of this timescale before detection.

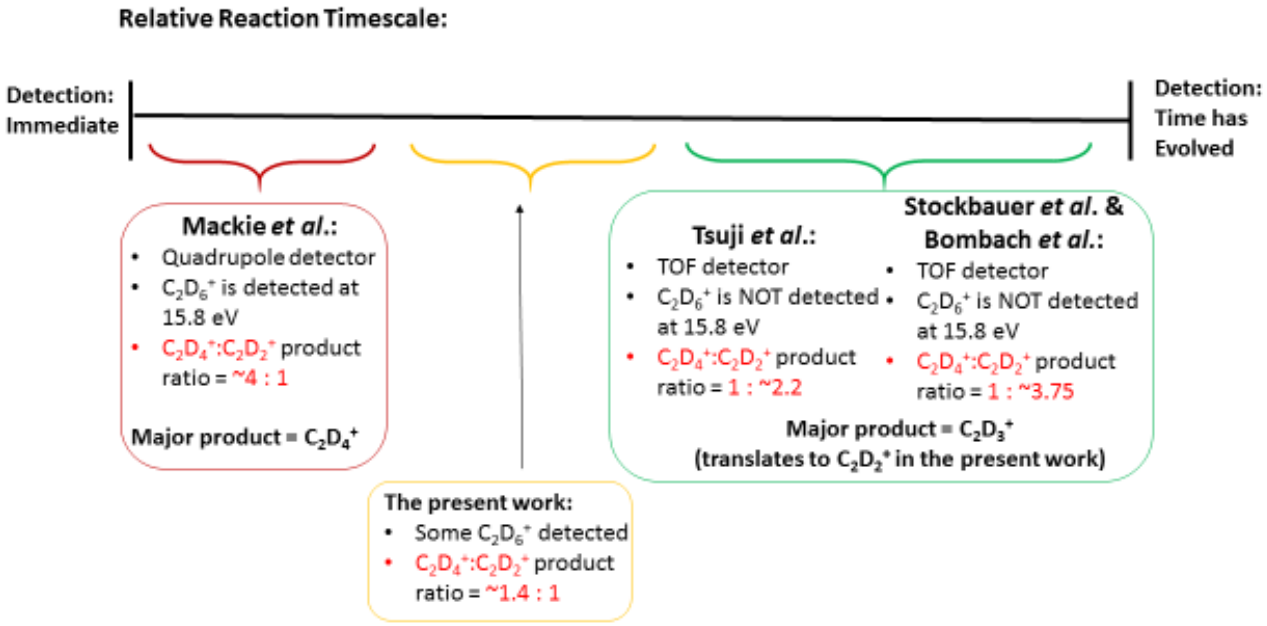

Figure 22: Diagrammatic representation of the difference in the timescales of our work in context with the related work with ethane ionization.

5.2 High ion-density conditions:

Experiments completed under high ion-density conditions, using the pin-anode, produced a variety of ionization products, as presented in the results section. As shown in Figure 7 in the results, a diverse product distribution is observed for experiments performed using a metal pin as the anode, even at a minimal ionization current. The presence of C_2D as a product was an important indicator that another process, in addition to CT, occurs in the EBMIS apparatus during experiments using the pin. The appearance energy of C_2D has been previously reported as 17.36 eV, which is a higher energy than is available in our experiments[42]. As mentioned earlier, the observed products, save C_2D, are thermodynamically allowed with Ar^+ charge-transfer ionization processes, however the branching ratios differ from previous research. Despite working at a lower energy than is required for C_2D production, the spectrum in Figure 12 in the results shows evidence that it is observed, as well as Figures 13 and 14 that show that the product appears in all experiments, at least to a minor extent, that were conducted using the pin-type of anode.

Under all ionization current conditions studied with the high ion-density configuration of the apparatus, C_2D_2 is the product with the highest relative yield. The branching ratio of C_2D_4:C_2D_2 is approximately $1 : (1.7 \pm 0.1)$, which is significantly different from the ratio of 1.4: 1 observed from the EBMIS experiment conducted under low ion-density conditions (using the plate-type anode). The ratio is closer to that predicted by the Tsuji *et al.*[33] and Bombach *et al.*[32] studies, however, the explanation for this shift in product distribution cannot be described in terms of timescales as before. The timescale for gas-phase decomposition in our EBMIS experiments remains the same since the sole change was the type of anode used for the set of experiments.

Instead, the deviations from the product distributions as presented earlier, as well as the presence of C_2D, can be rationalized through the proposal of dissociative recombination events.

When neutralization of the ionic fragmentation products, formed from initial CT ionization, occurs in the gas-phase, highly energized neutral species will be generated. The internal energy gained from the recombination of an ion with an electron in the gas-phase are close to the ionization energy of the neutral species, themselves, and can result in further fragmentation[43,44]. These processes, called dissociative recombination, could account for the branching ratios in the present work, provided that they occur prior to condensation into a matrix material. Dissociative recombination events that are able to occur prior to matrix formation in the EBMIS apparatus under these high ion-density experiments would result in products that are dehydrogenated to a greater extent.

In high ion-density conditions, the neutralizing electrons may encounter an ionic product of ethane ionization by charge transfer. As such, it is helpful to look at the possible dissociative recombination products available for each of the expected ethane ionization products that are detected after 15.8 eV ionization, as is the energy available in the present experiments. Under conditions that are optimal for dissociative recombination, an ethane cation would decompose into the fragments shown in Figure 23 below, showing branching ratios from the present experiments as well as the research by Plessis *et al.*[44]. The processes outlined below are described by tables of dissociative recombination data and adapted here for the ions expected for ethane ionization by Ar^+. This figure demonstrates that, following dissociative recombination, a shift in the ratio of C_2D_4:C_2D_2 is expected, however, there are no specific ratios predicted from this work.

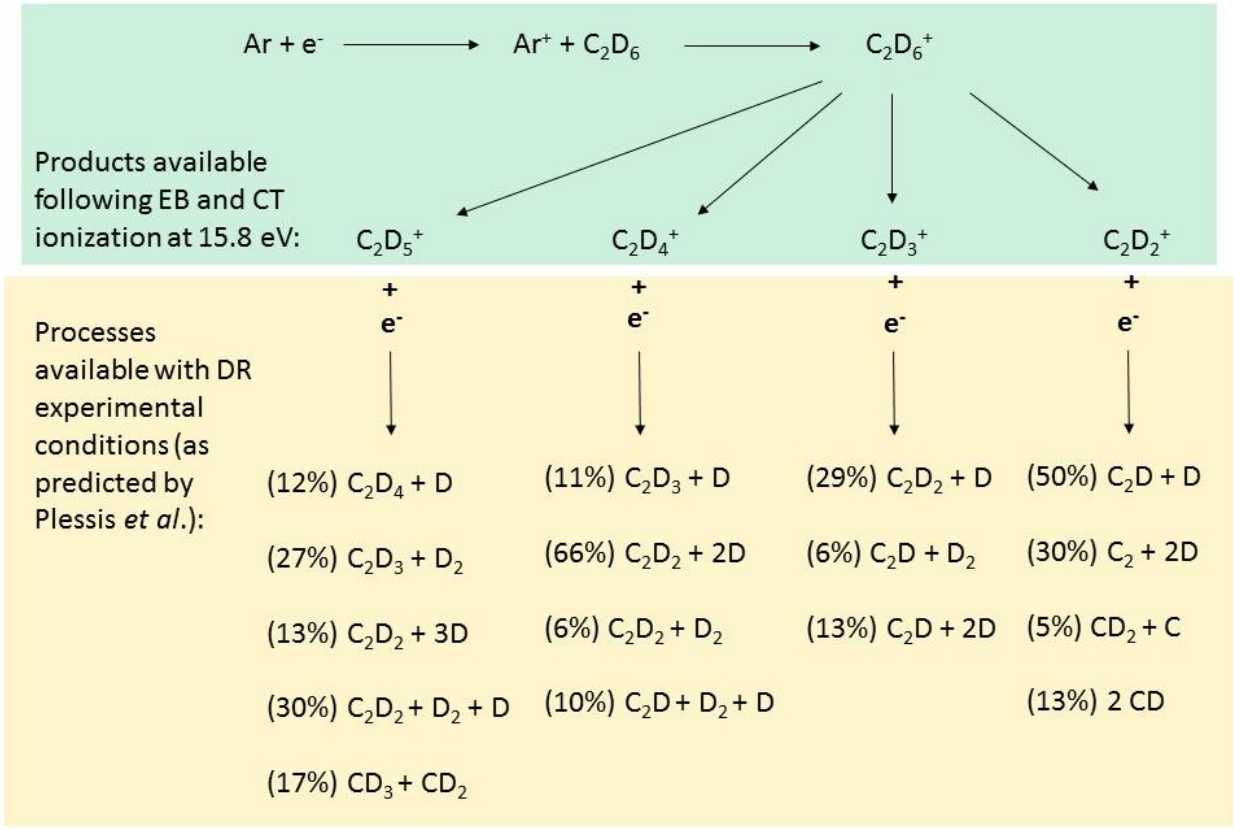

Figure 23: Predicted branching ratios for products of charge-transfer ionization of ethane via argon, which undergo dissociative recombination events upon formation under some conditions.

5.3 Influence of ionization current

In light of these mechanistic considerations, we can now revisit the influence of ionization current on the products observed. Figures 9 and 18 in the results section show that the fraction of ionized C_2D_6 precursor increases as the ionization current is increased. The consumption of precursor molecules is increased when the pin-anode is used, as compared to the plate-anode, for a particular ionization current. The results show that product distribution is also dependent on the ionization current of a particular experiment, to different effects, whether working in the high- or low-ion density regime.

When the plate anode is used, referred to as low ion-density experimental conditions, there is a linear increase in the yield of the major products, C_2D_4 and C_2D_2. Since there are no other species observed, even at the higher ionization currents, the type of chemical processes that occur are not changing and dissociative recombination events do not occur to an appreciable extent.

With use of the pin anode when high ion-density conditions are observed, however, dissociative recombination does occur, as discussed above. Varying the current for these high ion-density experiments changes the types of products observed, favoring dissociative recombination products at the highest measured currents. This dissociative recombination is responsible for the shift in products towards the increasingly dehydrogenated species, as the current is increased and the presence of high-energy electrons increases.

Table 2, below, presents the product ratio, C_2D_4:C_2D_2, for both the low and high ion-density conditions. In this table, the C_2D production is included with the C_2D_2 amounts, as both indicate the emergence of dissociative recombination events. First of all, the ratios in the table display the general trend that the major product observed changes depending on experimental conditions.

Under low ion-density experiments, when the plate-like anode is used, C_2D_4 is the major product, whereas there is a distinct shift to C_2D_2 as the major product in the high ion-density work, using the pin-like anode. The effect of changing the ionization current is also displayed in Table 2. It is shown that there is very little change in the overall product ratio in the low ion-density work, whereas there is a marked dependence on ionization current in the high ion-density work, where the product ratio favors the dehydrogenated products. Under high ion-density conditions, the ratio begins as a similar ratio found in the Tsuji *et al.*[33] work, to the ratio of nearly 1:5, C_2D_4:C_2D_2, as in the Stockbaeur *et al.*[31] and Bombach *et al.*[32] work.

Table 2: An analysis of the product ratio of C_2D_4:C_2D_2 under various electron flux conditions for both low ion-density (plate) and high ion-density (pin) experiments.

Electron Flux (μA)	Ratio (C_2D_4:C_2D_2): Low Ion-Density	Ratio (C_2D_4:C_2D_2): High Ion-Density
20	2.2 : 1	
30	1.0 : 1	1 : 2.1
40	2.5 : 1	
50	2.0 : 1	
60	1.0 : 1	1 : 2.9
70	1.8 : 1	
80	1.4 : 1	
90	1.4 : 1	1 : 3.75
120		1 : 4.3
150		1 : 5.2

5.4 Implications for acetone work

This ethane work has foundational implications for other work done using the EBMIS apparatus. It has become clear, here, that dissociative recombination events influence the chemistry observed in our experiments, depending on the experimental conditions. This work can be compared to published work concerning the ionization of acetone using the EBMIS apparatus following CT ionization at the same energy, 15.8eV[45]. In this acetone work, ethane, and associated dehydrogenated products, were identified following CT ionization from argon cation. The product CCCO is observed under conditions described in this thesis at high ion-density, with the production increasing as the ionization current is increased. The comparison to this acetone work demonstrates the reproducibility of the predictability of outcomes when moving from low ion-density experiments to high ion-density experiment where dissociative recombination is influential. This work also lends support to the conclusion that ethane cation is produced following ionization of acetone in the EBMIS apparatus. This is supported by the reproduction of linearity in the overall observations of each product under low ion-density (plate) and the shift in product distribution when moving into experimental parameters that favor dissociative recombination, as seen in the acetone results.

The EBMIS apparatus can be used to study ionization processes at a timescale intermediate to time of flight and quadrupole mass spectrometry experiments, as well as dissociative recombination studies of cations, by simply altering the anode used.

References

[1] Comita, P.B., Brauman, J.I. **1985.** *Science.* 227: 863-869; b) Lifshitz, C. **1987.** *Int. Rev. Phys. Chem.* 6(1):35-51

[2] See for example, Atkinson, R., Arey, J. **1994.** *Enviro. Heal. Persp*. 102(s4):117-127; Hudgins, D.M., Sandford, S.A. **1998.** *J. Phys. Chem. A.* 102:353-360

[3] Parnis J. M., King, K. A., Thompson, M. G. K. **2009.** *J. Mass Spec.* 44: 652-661.

[4] Robinson, P.J.; Holbrook, K.A. *Unimolecular Reactions*, Wiley-Interscience, New York, **1972.**

[5] Gross, J.H. Mass Spectrometry: A Textbook. **2004.** Springer-Verlag, Heidelburg, Germany

[6] Lorquet, J.C. **2000.** *Int. J. Mass Spec.* 200:43-56

[7] Brenton, A.G., Morgan, R.P., Beynon, J.H. **1979.** *Ann. Rev. Phys. Chem.* 30:51-78

[8] Rosenstock, H.M., Wallenstein, M.B., Wahrhaftig, A.L., Eyring, H. **1952.** *Proc. Nat. Acad. Sci.* 38: 667-678

[9] See, for example: Mirsaleh-Kohan, N., Robertson, W.D., Compton, R.N. **2008.** *Mass Spec. Rev.* 27:237-285; Nibbering, N.M.M. **2006.** *Mass Spec. Rev.* 25:962-1017

[10] Hammerum, S., Norrman, K., Solling, T.I., Anderson, P.E., Jensen, L.B., Vulpius, T. *J. Am. Chem. Soc.* **2005.** 127, 6466

[11] Baer, T. **2000.** *Int. J. Mass Spec.* 200:443-457; Ng, C.Y. **2000.** *Int. J. Mass Spec.* 200:357-386

[12] Whittle, E., Dows, D.A., Pimentel, G.C. **1954.** *J. Chem. Phys.* 22: 1943

[13] Andrews, W.L., Pimentel, G.C. **1966.** *J. Chem. Phys.* 44(6):2361-2369

[14] Lin, C.Y., Krantz, A. **1972.** *J. Chem. Soc. Chem. Comm.* 1111-1112, 1316; Chapman, O.L., McIntosh, C.L., Pacansky, J. **1973.** *J Am Chem Soc.* 95:244-246; Pong, R.G.S., Shirk, J.S. **1973.** 95:248-249

[15] Dunkin, I.R. Matrix Isolation Techniques: A Practical Approach. Oxford, New York. **1998.**

[16] Silverstein, R.M., Webster, F.X., Kiemle, D.J. Spectrometric Identification of Organic Compounds, 7th Ed. Wiley, New York**, 2005**.

[17] Nakamoto, K. Infrared and Raman Spectra of Inorganic and Coordination Compounds. Part A, B. 5th Ed. Wiley, New York, **1997.**

[18] Milligan, D.E.; Jacox, M.E.; Guillary, W.A. *J. Chem. Phys.*, **1970,** 52, 3864

[19] Breeze, P.A.; Burdett, J.K.; Turner, J. *J. Inorg. Chem.* **1981,** 20, 3369.

[20] Knight, L.B.; Bostick, J.M.; Woodward, R.W.; Steadman, J. *J. Chem. Phys.*, **1983.** 78, 6415.

[21] Suzer, S.; Andrews, L. *J. Chem. Phys.* **1988,** 88, 916.

[22] Suzer, S.; Andrews, L. *Phys. Lett*. **1988.** 150, 13

[23] Szczepanski, J.; Roser, D.; Personette, W.; Eyring, M.; Pellow, R.; Vala, M. *J. Phys. Chem.* **1992,** 96, 7876.

[24] Zhang, X.K.; Lewars, E.G.; March, R.E.; Parnis, J.M. *J. Phys. Chem.* **1993,** 97, 4320.

[25] Parnis, J.M.; Hoover, L.E.; Fridgen, T.D.; Lafleur, R.D. *J. Phys. Chem.* **1993**, 97, 10708

[26] Zhang, X.K.; Parnis, J.M.; Lewars, E.G.; March, R.E. *Can. J. Chem.* **1997,** 75, 276.

[27] Fridgen, T.D.; Parnis, J.M. *J. Phys. Chem.* **1997**, 101, 5117

[28] Lias, S. G.; Bartress, R.E.; Liebman, J. F.; Holmes, J.L.; Levin, R. D.; Mallard, W. *J. Phys. Chem. Ref. Data,* **1988,** 17, Supplement 1. Jacox, M. E. *Rev. Chem. Intermed.* **1978,** 2, 1.

[29] Thompson, M.G.K.; Parnis, J.M. *J. Phys. Chem.* **2008,** 112, 12109.

[30] See for example: Shoen, R.I. *J. Chem. Phys.* **1962,** 37, 2032. Prasil, Z.; Forst, W. *J. Phys Chem.* **1967,** 71 3166. Chupka, W.A.; Berkowitz, J. *J. Chem. Phys.* **1967,** 47**,** 2921. Rabalais, J. W.; Katrib, A. *Mol. Phys.* **1974**, 27, 923. Guthe, F.; Malow, M.; Weitzel, K.-M.; Baumgartel, H. *Int J. Mass Spec.* **1998.** 172, 47.

[31] Stockbauer, R. *J. Chem. Phys.* **1973,** 58, 3800.

[32] Bombach, R.; Dannacher, J.; Stadelmann, J-P. *Int J Mass Spec.* **1984,** 58, 217

[33] Tsuji, M.; Kouno, H.; Matsumura, K-I.; Funatsu, T. *J. Chem. Phys.* **1993,** 98, 2011

[34] Mackie, R.A.; Sands, A.M.; Scully, S.W.J.; Holland, D.M.P.; Shaw, D.A.; Dunn, K.F.; Latimer, C.J. *J Phys B.* **2002**, 35, 1

[35] Szczepanski, J.; Roser, D.; Personette, W.; Eyring, M.; Pellow, R.; Vala, M. *J. Phys. Chem.* **1992,** 96, 7876.

[36] Dunkin, I.R. *Matrix Isolation Techniques: A practical approach.* Edited by Harwood L.M. and Moody, C.J. Oxford University Press Inc., New York, USA, **1998.**

[37] Bomem GRAMS_32, Version 4.14. Galactic Industries Corporation. 1996.

[38] Gaussian 03, Revision C.01 Frisch, M. J.; Trucks, G. W.; Schlegel, H. B.; Scuseria, G. E.; Robb, M. A.; Cheeseman, J.R.; Montgomery, Jr., J. A.; Vreven, R.; Kudin, K. N.; Burant, J. C.; Millam, J. M.; Iyengar, S. S.; Tomasi, J.; Barone, V.; Mennucci, B.; Cossi, M.; Scalmani, G.; Rega, N.; Petersson, G. A.; Nakatsuji, H.; Hada, M.; Ehara, M.; Toyota, K.; Fukuda, R.; Hasegawa, J.; Ishida, M.; Nakajima, R.; Honda, Y.; Kitao, O.; Nakai, H.; Klene, M.; Li, X.; Know, J. E.; Hratchian, H. P.; Cross, J. B.; Bakken, V.; Adamo, C.; Jaramillo, J.; Gomperts, R.; Stratmann, R. E.; Yazyev, O.; Austin, A J.; Cammi, R.; Pomelli, C.; Ochterski, J. W.; Ayala, P. Y.; Morokuma, K.; Voth, G. A.; Salvador, P.; Dannenberg, J. J.; Zakrewski, V. G.; Dapprich, S.; Daniels, A. D.; Strain, M. C.; Farkas, O.; Malick, D. K.; Rabuck, A. D.; Raghavachari, K.; Foresman, J. B.; Ortiz, J. V.; Cui, Q.; Baboul, A. G.; Clifford, S.; Cioslowski, J.; Stefanov, B. B.; Liu, G.; Liashenko, A.; Piskorz, P.; Komaromi, I.; Martin, R. L.; Fox, D. J.; Keith, T.; Al-Laham, M. A.; Peng, C. Y.; Nanayakkara, A.; Challacombe, M.; Gill, P. M. W.; Johnson, B.; Chen, W.; Wong, M. W.; Gonzalez, C.; and Pople, J. A. Gaussian, Inc, Wallingford CT, 2004.

[39] GaussView, Version 3.09, Dennington II, Roy; Keith, Todd; Millam, John; Eppinnett, Ken; Hovell, W. Lee; and Gilliland, Ray. Semichem, Inc., Shawnee Mission, KS, 2003.

[40] Shepherd, R.A.; Graham, R.M. *J Chem Phys.* **1987**, 86 (5), 2600, and Jacox, M.E.; Olson, W.B. *J Chem Phys*. **1987**, 86, 3134

[41] Oehlschlaeger, M.A.; Davidson, D.F.; Hanson, R.K. *Proc Combust Inst.* **2005**, 30, 1119; and Davidson, D.F.; Di Rosa, M.D.; Hanson R.K.; Bowman, C.T. *Int J Chem Kin.* **1993**, 29, 969

[42] Shepherd, R.A.; Graham, R.M. *J Chem Phys.* **1987**, 86 (5), 2600; and Jacox, M.E.; Olson, W.B.; *J Chem Phys.* **1987**, 86, 3134

[43] Kokouline, V.; Douget, N.; Greene, C.H. *Chem Phys Lett.* **2011,** 507, 1

[44] Plessis, S.; Carrasco, N.; Pernot, P. *J Chem Phys.* **201**0, 133, 134110

[45] Parnis, J.M.; King, K.A.; Thompson, M.G.K. *J Mass Spec* **2013.** 48, 1224

Statement of Original Contribution

I, Kaitlynn King, hereby declare that the work presented in this thesis is original content conducted and written by myself. This work was published in the Journal of Mass Spectrometry prior to the publication of this thesis, a paper which I helped to write. The reference to this paper is as follows:

Parnis, J.M., King, K.A., Campbell, S.E., and Thompson, M.G.K. Ethane cation decomposition characterization by EBMI spectroscopy: gas-phase dissociative recombination as a source of secondary products. *J. Mass Spec.* **2012.** *47*, 89.